

# GEOCHEMICAL AND Sr-Nd-Pb ISOTOPIC CHARACTERISTICS OF EXTRUSIVE ROCKS WITHIN THE ÇETMI OPHIOLITIC MELANGE, BIGA PENINSULA

Aykut Güçtekin 

Department of Geology, University of Kocaeli, İzmit, Turkey.

 Corresponding author, email: a\_guctekin@yahoo.com

**Keywords:** *Çetmi Ophiolitic Mélange, Sr-Nd-Pb isotopes, back-arc basin basalts, mantle metasomatism, Intra-Pontide suture zone, Turkey.*

## ABSTRACT

The different geochemical characteristics of the extrusive rocks of the Çetmi Ophiolitic Mélange (ÇOM) a remnant of the Intra-Pontide Suture (IPS) in the Biga Peninsula, NW Turkey, evidence the episodic formation of oceanic crust. Geochemically, volcanic rocks are divided into three groups: ocean island basalts (OIB), enriched mid-ocean ridge basalts (E-MORB) and basalts with supra-subduction zone (SSZ) affinity. While the OIB type samples were produced by small degrees partial melting from an enriched source, the E-MORB type samples point to mixing of enriched and depleted sources. In the OIB-type samples, the depletion of Zr and Hf compared to Nd as well as enrichment of Nb-Ta are attributed to presence of the amphibole in the mantle source. Radiogenic Pb isotope compositions towards EMII support metasomatic processes related to fractionation in the mantle reservoir. The SSZ samples are characterized by enriched light rare earth elements (LREE) and depleted high field strength elements (HFSE). The trace element characteristics of the SSZ samples indicate that a depleted MORB mantle source interacted with subduction-derived fluids due to the slab dehydration processes. Besides, the Sr-Nd-Pb isotope characteristics suggest that these samples originated from a MORB-type mantle source metasomatized by fluids or melts from subducted sediments. The major, trace element and isotopic data of the volcanic rocks in the ÇOM indicate that the oceanic lithosphere is generated along a SSZ-type spreading centre at an arc-basin system within the Intra-Pontide Ocean.

## INTRODUCTION

Ophiolites are remnants of oceanic lithosphere formed at mid-ocean ridges and in marginal sea basins (pre-arc, fore-arc or backarc basins) (e.g., Dilek and Furnes, 2011). The magmatic products in the crustal parts of ophiolites can provide significant information on the melt generation at different stages of evolving lithosphere. The geochemical characteristics of the basic volcanic rocks forming the crustal part of the oceanic lithosphere can yield critical information concerning the original tectonic setting of the ophiolite complexes. These characteristics are controlled by parameters such as the rate of seafloor spreading, geometry of ridge system, the proximity of a spreading centre to a plume or a trench, the mantle composition, temperature and fertility during partial melting, and the availability of fluids (Dilek and Furnes, 2014). Additionally, they also contribute to the interpretation of the time-dependent evolution of arc-basin systems in the formation of the oceanic crust (Shervais, 2001; Pearce, 2003).

The focus of this study, the Çetmi Ophiolite, is located within the Biga Peninsula in northwest Anatolia (Kaaden, 1959; Bingöl et al., 1975; Okay et al., 1990; 1996; Ercan et al., 1995; Pickett and Robertson, 1996; Beccalotto, 2003). The ophiolite is part of the Intra-Pontide Suture (IPS) Zone, i.e. one of the branches of the Neotethys Ocean (Fig. 1a; Şengör and Yılmaz, 1981) that lies between the Istanbul-Zonguldak terrane to the north and the Sakarya terrane to the south of Anatolia (e.g., Göncüoğlu et al., 1997; 2000). The area is composed of rocks with diverse age and origins derived from deformed and/or metamorphic units and ophiolites originated from the closure of the Neotethys oceanic basin (e.g., Göncüoğlu et al., 2008). The IPS Zone, its geological setting, age and evolution have been previously discussed by many researchers (e.g., Göncüoğlu and Eréndil,

1990; Yılmaz et al., 1997; Elmas et al., 1997; Yiğitbaş et al., 1999; Robertson and Ustaömer, 2004; Akbayram et al., 2012). This whole zone, in the Biga Peninsula is described as Çetmi Ophiolitic Mélange (ÇOM). The ÇOM has a complex internal structure and emplaced the region as the remnant of the Intra-Pontide Ocean during Late Cretaceous (e.g., Okay, 1987; Okay et al., 1990).

These mélanges usually occur in the oceanic trenches when tectonic deformation mixes rocks chaotically (Hamilton, 1969; Dewey and Bird, 1971; Hall, 1976). Even though the mélanges are widely distributed, their recognition, origin, deformation mechanism and tectonic meaning have always been controversial (Silver and Beutner, 1980; Raymond and Terranova, 1984). The study of magmatic rocks in the ÇOM helps understanding the magmatic and geodynamic evolution of the ophiolites in the IPS Zone. Previous studies indicated that basalts of the mélange were originated in volcanic arc or within plate environment (Beccalotto, 2003). This study aims to decipher the nature of mantle source, geodynamic environment and the Intra-Pontide oceanic crust evolution by using whole-rock major, trace and REE and Sr-Nd-Pb isotopic data determined on the ÇOM volcanic rocks in the Biga Peninsula.

## GEOLOGICAL SETTING

The Biga Peninsula in NW Anatolia is located to the west of the Sakarya terrane, south of the Rhodope and Serbo-Macedonian massifs in Greece and the Thrace Tertiary basin (Fig. 1a; Okay et al., 1990). It displays a complex geology containing a wide variety of metamorphic, magmatic and sedimentary rock units. There are four different tectonic zones, i.e., Gelibolu, Ezine, Ayvacık-Karabiga and Sakarya from NW to SE in the Gelibolu and Biga Peninsulas. The

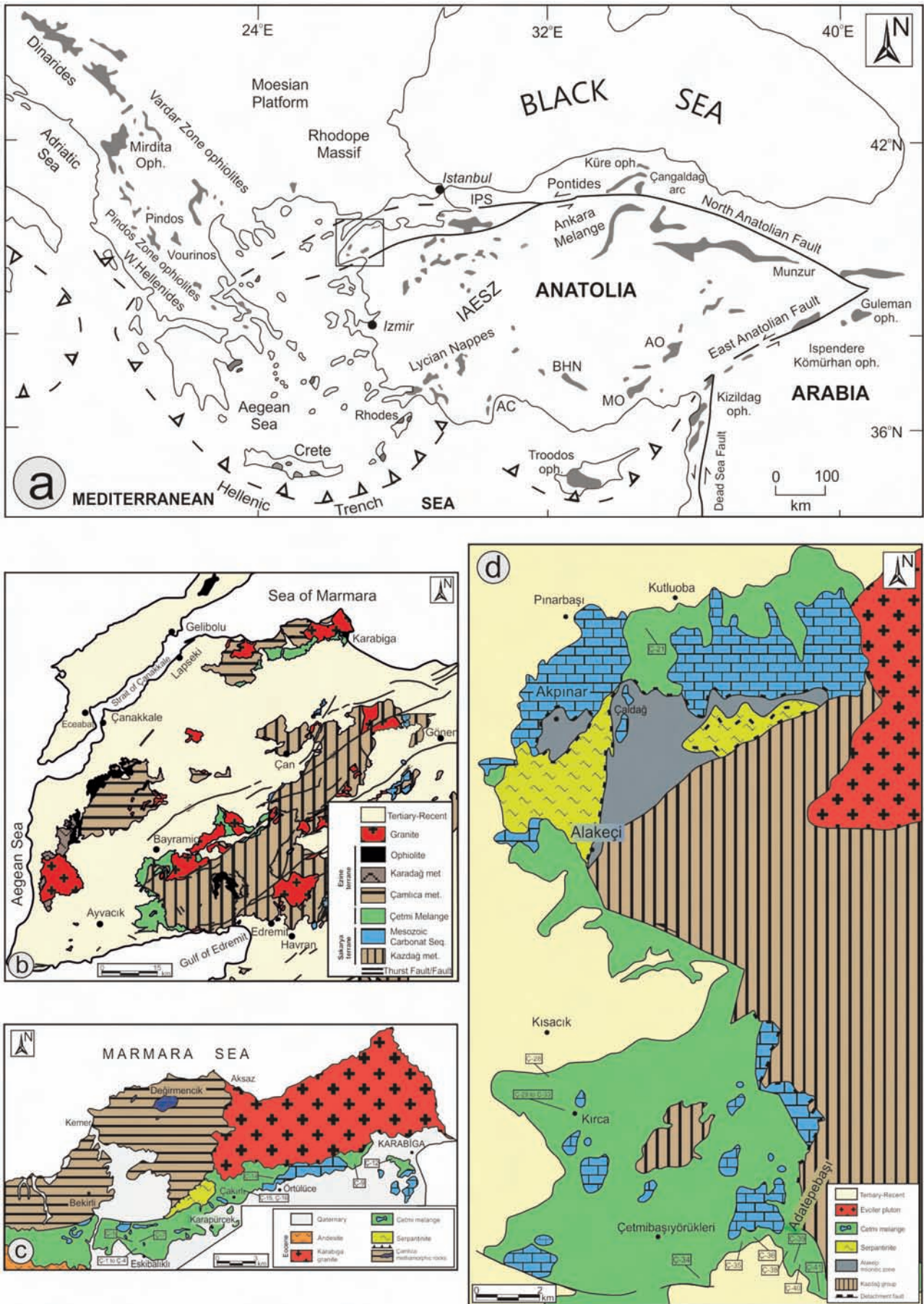


Fig. 1 - a) Distribution of Neotethyan ophiolites in the Eastern Mediterranean region (Dilek and Flower, 2003); b) Geological map of the Biga Peninsula (simplified from Okay and Satır, 2000a); c, d) Geological map and sample locations of the northern and southern Çetmi Mélange, respectively (Beccaletto et al., 2005).

basement of the Çetmi Ophiolite is composed of the Kazdağ Metamorphic Complex, Karakaya Complex - Ezine Group, Çamlıca and Kemer metamorphics and pre-Late Cretaceous ophiolitic rocks (Fig. 1b; Okay et al., 1990).

Lithological units of the ÇOM includes spilites, greywackes, pelagic shales, serpentinites and radiolarites (Okay, 1987; Okay et al., 1990). The greywacke-shales are always found in tectonic contact with other lithologies, and form the *mélange* matrix. This association crops out between Boztepe-Çetmibaşıyörükleri to the north, in the north of Eskibalıklı, and Kırca to the south (Beccalotto, 2003). The Çetmi *Mélange* is located in the two different regions of the west of Karabiga in the north of the Biga Peninsula (Fig. 1c) and between Bayramiç and Küçükkuyu in the south (Fig. 1d; Beccalotto et al., 2005, Aygün et al., 2012). The volcanic rocks, which are the most common lithology of the *mélange* in both regions, are spilitic and occur as tectonic slices (Okay et al., 1990). In some sections, sheet flows with massive volcanic structure can be explained by higher effusion rates compared to the formation of pillow lavas. Various limestone blocks from Late Triassic to Late Cretaceous are also identified in tectonic contact with the spilitic basalts (Beccalotto, 2003).

The *mélange* crops out in the western part of Karabiga, Karapürçek Village, Hacidede and Kız Hills, and tectonically overlies the Çamlıca Metamorphics. (Fig 1c). The Karabiga Granitoids cuts the *mélange* intrusively. Where the granitoids are intruded into limestones, contact metamorphism results in skarn formation and crystallization of garnet, pyroxene and epidote associated with large calcite crystals. (e.g., Güçtekin et al., 2004). In addition, sandstone-shale alternations, radiolarite-chert and serpentinite slices are observed in the *mélange*. Partly spilitic volcanic rocks form large part of the *mélange* in Eskibalıklı, north of Çakırlı and in west of Karabiga (Okay et al., 1990; Beccalotto, 2003). These volcanics are dark green to black fine-grained massive rocks with widespread fracturation and occurrence of amygdalae.

North of Küçükkuyu, the *mélange* is commonly found west of the metamorphic rocks belonging to the Kazdağ Metamorphic Complex and displays a complex and imbricated inner structure (Fig. 1d). Here, *mélange* slices are bounded by NE-trending steeply dipping faults. Spilitic basalts and pyroclastic rocks are accompanied by Late Triassic, Late Jurassic-Early Cretaceous and Late Cretaceous limestone blocks, shales and greywackes with minor serpentinite, radiolarian chert, garnet micaschist and eclogite slices (Okay et al., 1990). Late Oligocene-Miocene magmatic rocks both cut and overlie the Çetmi *Mélange* in this area. The volcanic rocks of *mélange* are found as tectonic slices south of Kutluoba, south of Kırca and north of Küçükkuyu, where they mimic the outcrops observed at west in Karabiga (Beccalotto, 2003).

Beccalotto et al. (2005) obtained six different radiolaria ages from deep water sediments in the Çetmi *Mélange* from late Bajocian to Aptian. The origin of the *mélange* was previously attributed to the Intra-Pontide Ocean (Şengör and Yilmaz, 1981).

## PETROGRAPHY

The extrusive rocks of the Çetmi *Mélange* are basalts, basaltic andesites and alkali basalts. Although basalts and basaltic andesites are mineralogically and texturally indistinguishable, they are identified based on Nb/Y vs. Zr/Ti ratios

(Fig. 2a). Basalts and basaltic andesites have dominantly aphyric, hyalopilitic and pylotaxitic and rarely weakly porphyritic textures. Plagioclase and clinopyroxenes are main phases, and olivine, orthopyroxene and Fe-Ti oxide minerals are minor phases. Modal abundances of phenocrysts of samples are ~50-55 vol% plagioclase, ~25-30 vol % clinopyroxene, ~8-10 vol % orthopyroxene, ~3-5 vol % olivine, and ~4-6 vol% Fe-Ti oxide. Pyroxenes occur as small euhedral/subhedral phenocrysts compared to plagioclase; they sometimes display oscillatory zoning. The groundmass consists of plagioclase, clinopyroxene, Fe-Ti oxide. The samples also contain albite, chlorite, epidote, quartz, calcite, actinolite and iron oxide minerals, which are by-products of sea-floor hydrothermal alteration. Fractures and vesicles generally are filled with calcite and fibrous chlorite.

Intergranular and intersertal textures are generally observed in alkali basalts. The ratio of phenocrysts to matrix is up to 25%. Phenocrysts, in decreasing order of abundance, consist of plagioclase (~ 46 vol%), clinopyroxene (~ 37 vol%), olivine (~ 16 vol%) and Fe-Ti oxides (~ 3 vol%). Olivine phenocrysts are euhedral to subhedral, minor rounded olivine is ~ 1 mm across. Glomeroporphyritic clusters of plagioclase, pyroxene and olivine also occur. Seafloor hydrothermal alteration of basalts resulted in overprint of primary phases by secondary minerals. This process caused formation of sericite and carbonate in plagioclases, uraltization of pyroxenes and serpentinitization of olivines. The volcanics commonly show carbonates filling the cracks and fibrous chlorite fillings the vesicles.

## Analytical techniques

A selected set of 25 relatively fresh samples were analyzed at ACME Analytical Laboratories Vancouver (Canada) to determine major and trace-element compositions. 0.2 g of rock-powder was fused with 1.5 g LiBO<sub>3</sub> and dissolved in 100 ml 5% HNO<sub>3</sub>. Loss on ignition (LOI) was determined on the dried samples heated to a temperature of 1000 °C. Rare earth elements (REE) analyses were performed by ICP-MS at ACME. Detection limits ranged from 0.01 to 0.1 wt% for major oxides, from 0.1 to 10 ppm for trace elements, and from 0.01 to 0.5 ppm for REE. The major and trace element contents and the sample locations are given in Table 1.

Eight samples were also analyzed at the Radiogenic Isotope Laboratory of the METU Central Laboratory to determine Sr-Nd isotopic compositions following procedures given in Köksal and Göncüoğlu, (2008). Isotope ratios were measured using a Triton Multi-Collector Thermal Ionization Mass Spectrometer. Analytical uncertainties are given at 2-sigma level. The USGS reference material BCR-1 resulted in <sup>87</sup>Sr/<sup>86</sup>Sr = 0.705014±5 and 143Nd/144Nd = 0.512638±4. Seven of the samples analysed for Sr-Nd isotope compositions were also tested for Pb isotope ratios at the Laboratoire G-Time at the Department of Earth and Environmental Sciences of the "Université Libre de Bruxelles" (Belgium). To remove alteration and any potential contamination, a leaching procedure was applied to powdered whole rock samples (250 mg), with repeated additions of 6N sub-boiled HCl (5-6 times) followed by 30-minutes ultrasonic baths until the solution was clear. The reference values are from Weiss et al. (2006). Analyses of the SRM981 Pb standard solution were performed and yielded <sup>208</sup>Pb/<sup>204</sup>Pb = 36.7174±47 (2σ), <sup>207</sup>Pb/<sup>204</sup>Pb = 15.4978±13 (2σ), and <sup>206</sup>Pb/<sup>204</sup>Pb = 16.9408±20 (2σ).

Table 1 - Whole-rock major and trace element compositions of the volcanic rocks from the ÇOM.

Sample No	C-1	C-2	C-3	C-4	C-5	C-7	C-9	C-12	C-21	C-28	C-29	C-30	C-31
Longitude	27° 05' 56" E	27° 05' 49" E	27° 05' 48" E	27° 05' 41" E	27° 05' 38" E	27° 06' 01" E	27° 16' 40" E	27° 17' 18" E	26° 34' 54" E	26° 32' 10" E	26° 33' 11" E	26° 33' 11" E	26° 33' 11" E
Latitude	40° 20' 53" N	40° 20' 54" N	40° 20' 53" N	40° 20' 57" N	40° 20' 59" N	40° 20' 09" N	40° 23' 32" N	40° 23' 59" N	39° 45' 56" N	39° 18' 14" N	39° 37' 35" N	39° 37' 38" N	39° 37' 38" N
Rock type	B. andesite	Basalt	Basalt	B. andesite	Basalt	Basalt	Basalt	B. andesite	B. andesite	Basalt	Basalt	Basalt	Basalt
Magmatic affinity	SSZ												
SiO <sub>2</sub>	56.23	56.08	55.70	49.66	51.75	51.91	52.44	56.75	58.12	49.68	51.77	49.12	52.01
TiO <sub>2</sub>	0.87	1.06	1.09	0.45	0.91	0.46	0.67	0.59	0.36	0.93	0.86	0.75	0.95
Al <sub>2</sub> O <sub>3</sub>	15.91	15.58	15.82	16.93	17.30	14.85	13.85	17.06	15.52	15.62	15.06	16.38	15.06
Fe <sub>2</sub> O <sub>3</sub>	11.43	10.52	9.61	9.75	11.52	9.05	6.98	9.95	9.99	13.17	10.61	9.81	11.77
MnO	0.06	0.16	0.15	0.19	0.22	0.16	0.31	0.10	0.04	0.25	0.18	0.19	0.17
MgO	2.96	2.40	3.43	5.36	2.61	4.70	3.74	2.59	3.05	3.93	4.12	5.45	4.44
CaO	4.46	6.18	6.51	11.36	8.45	9.38	15.50	0.70	3.30	4.25	4.79	5.11	4.19
Na <sub>2</sub> O	5.47	5.51	5.30	3.73	4.54	3.19	3.59	4.96	4.16	5.83	6.08	5.29	6.15
K <sub>2</sub> O	0.61	0.58	0.54	0.45	0.99	0.50	1.33	4.12	4.19	0.49	0.52	1.22	0.16
P <sub>2</sub> O <sub>5</sub>	0.20	0.16	0.16	0.11	0.21	0.13	0.10	0.38	0.10	0.28	0.14	0.16	0.15
LOI	1.7	1.6	1.5	1.7	1.3	5.4	1.4	2.6	2.0	5.40	5.70	6.30	4.70
Total	99.91	99.80	99.81	99.78	99.76	99.77	99.86	99.81	99.84	99.80	99.81	99.75	99.79
V	117	320	340	287	345	312	141	126	9	212	314	251	400
Co	6.5	18.9	22.5	24.3	29.2	32.0	19.5	11.4	4.1	25.3	29.3	26.4	27.6
Ga	12.3	16.1	16.0	16.8	18.1	15.2	11.4	15.1	20.8	20.4	15.3	16.8	14.3
Rb	16.0	6.9	11.2	13.6	15.8	9.5	20.8	54.5	94.7	18.7	12.0	14.9	3.5
Sr	141.6	241.2	180.2	319.8	330.1	340.8	179.2	145.5	125.4	167.4	186.5	197.6	123.8
Y	35.0	27.4	27.3	18.7	24.1	12.7	18.1	25.9	32.3	34.3	18.5	18.5	18.3
Zr	129.0	92.4	92.4	53.0	59.8	50.7	52.1	126.5	183.8	99.3	63.5	77.8	57.9
Nb	11.0	7.2	7.8	3.7	5.2	3.1	5.9	9.8	14.8	9.6	5.2	6.9	4.3
Cs	0.8	1.9	1.7	2.3	1.6	1.2	0.9	0.6	0.8	11.3	6.6	4.9	1.4
Ba	100	144	171	110	300	158	83	483	764	208	113	380	67
La	19.6	16.3	16.5	28.4	17.4	22.2	13.3	36.5	35.8	25.8	11.6	16.6	11.5
Ce	41.7	29.5	28.9	47.4	31.9	40.1	24.1	64.1	67.1	52.2	22.4	30.4	22.8
Pr	5.52	3.79	3.79	5.85	3.88	4.48	3.00	7.65	8.02	6.32	2.90	3.45	2.78
Nd	22.8	15.6	15.9	23.1	16.6	15.7	11.7	28.5	30.5	24.8	11.0	14.4	11.9
Sm	5.27	3.97	3.99	4.59	3.71	2.98	2.67	5.41	6.05	5.21	2.98	3.20	2.96
Eu	1.62	1.26	1.19	1.30	1.21	0.80	0.74	1.50	1.41	1.65	0.97	0.89	0.88
Gd	6.28	4.20	4.78	4.18	4.41	3.17	2.99	5.32	6.39	6.07	3.37	3.53	3.21
Tb	1.05	0.75	0.83	0.63	0.69	0.40	0.44	0.79	0.91	0.94	0.58	0.61	0.54
Dy	6.51	4.84	5.42	3.61	4.41	2.46	2.75	4.45	5.67	5.97	3.47	3.64	3.45
Ho	1.28	1.02	1.09	0.66	0.94	0.50	0.57	0.88	1.04	1.18	0.70	0.78	0.69
Er	3.33	3.05	3.42	1.99	2.93	1.56	1.70	2.63	3.37	3.55	2.33	2.33	2.25
Tm	0.49	0.46	0.51	0.28	0.41	0.23	0.24	0.39	0.48	0.51	0.32	0.35	0.34
Yb	3.29	3.05	3.36	1.85	2.71	1.64	1.50	2.66	3.24	3.48	2.31	2.37	2.25
Lu	0.49	0.48	0.50	0.27	0.42	0.24	0.24	0.40	0.49	0.51	0.35	0.35	0.33
Hf	5.6	2.5	2.7	1.7	1.8	1.5	1.5	2.8	6.9	3.6	1.7	2.2	1.7
Ta	0.6	0.4	0.3	0.3	0.3	0.2	0.3	0.6	0.9	0.5	0.4	0.5	0.3
Th	6.9	3.4	3.4	11.1	3.1	7.8	2.4	6.1	14.0	6.7	2.7	3.8	2.2
U	1.2	1.0	1.1	0.4	1.3	2.4	1.1	2.9	3.4	1.6	1.6	1.4	1.0
Eu/Eu*	0.86	0.94	0.83	0.90	0.91	0.80	0.80	0.85	0.69	0.89	0.94	0.81	0.87
Mg#	33.9	31.1	41.4	52.1	31.0	50.7	53.0	34.0	37.7	37.2	43.5	52.4	42.8

### Effects of alteration

The samples show low to high loss on ignition values (LOI: 0.6-9.7 wt%, Table 1), clearly reflecting presence of hydrothermal overprint recognized during petrographic investigation. Although this alteration can mobilize some of the major as well as the LILE elements (Ba, Rb, Th, Sr, U and K), HFS elements (Y, Zr, Nb, Ta, Ti and REE) may be considered immobile (Pearce and Cann, 1973; Floyd and Winchester, 1978). Thus, in order to discuss geochemical and petrogenetic characteristics of the investigated volcanic rocks, we considered REE and HFSE concentrations.

### Major and trace element compositions

The SiO<sub>2</sub> contents of the volcanic rocks range from 48.20 to 58.11%. In the Nb/Y vs. Zr/Ti diagram (Pearce, 1996), the samples fall into the alkaline basalt, basalt and basaltic andesite areas (Fig. 2a). Some of the samples in the Nb/Y-Zr/(P<sub>2</sub>O<sub>5</sub>\*10.000) diagram (Fig. 2b; Floyd and Winchester, 1975) display an alkaline affinity. Immobile trace element ratio of Zr vs. Y (Fig 2b; after Ross and Bedard, 2009) indicates a calc-alkaline to transitional trend for sub-alkaline volcanic rocks. In Zr-Th-Nb ternary plot (Wood, 1980), some samples are also classified as within-plate OIB, while others

Table 1 (continued)

Sample No	C-32	C-33	C-34	C-35	C-38	C-41	C-16	C-36	C-39	C-40	C-14	C-15
Longitude	26° 33'	26° 33'	26° 34'	26° 37'	26° 38'	26° 38'	27° 10'	26° 37'	26° 38'	26° 38'	27° 11'	27° 10'
	07" E	07" E	14" E	26" E	01" E	42" E	56" E	40" E	05" E	07" E	35" E	59" E
Latitude	39° 37'	39° 37'	39° 35'	39° 35'	39° 35'	39° 34'	40° 22'	39° 35'	39° 35'	39° 35'	40° 23'	40° 22'
	39" N	39" N	00" N	36" N	25" N	53" N	49" N	36" N	23" N	25" N	07" N	50" N
Rock type	Basalt	Basalt	Basalt	B.andesite	Basalt	B.andesite	A.basalt	A.basalt	A.basalt	A.basalt	Basalt	Basalt
Magmatic affinity	SSZ	SSZ	SSZ	SSZ	SSZ	SSZ	OIB	OIB	OIB	OIB	E-MORB	E-MORB
SiO <sub>2</sub>	51.47	51.30	48.41	58.11	53.75	59.02	47.75	51.47	48.12	49.40	44.05	48.20
TiO <sub>2</sub>	0.92	0.96	0.78	0.61	0.83	0.70	1.68	2.08	1.64	2.70	1.16	1.10
Al <sub>2</sub> O <sub>3</sub>	14.33	15.19	15.40	16.79	16.29	16.62	19.54	16.86	17.24	16.31	15.41	17.24
Fe <sub>2</sub> O <sub>3</sub>	12.20	12.17	8.18	5.55	8.53	6.98	9.05	9.02	8.76	13.03	10.61	9.80
MnO	0.16	0.17	0.15	0.07	0.15	0.03	0.12	0.12	0.16	0.10	0.21	0.15
MgO	4.78	3.85	4.62	1.52	4.90	2.28	3.87	4.33	6.61	3.76	7.48	6.15
CaO	6.88	7.34	9.25	4.63	8.70	2.20	13.21	3.22	6.71	3.54	18.18	12.09
Na <sub>2</sub> O	3.56	2.84	2.10	3.47	2.69	2.51	2.82	5.14	4.18	4.50	1.21	3.26
K <sub>2</sub> O	1.01	1.46	1.01	3.33	1.34	5.06	0.46	1.87	1.89	1.20	0.60	0.38
P <sub>2</sub> O <sub>5</sub>	0.11	0.16	0.15	0.17	0.15	0.16	0.24	0.39	0.32	0.44	0.16	0.09
LOI	4.30	4.30	9.70	5.50	2.40	4.30	1.0	5.30	3.80	4.70	0.6	1.3
Total	99.76	99.75	99.75	99.78	99.75	99.81	99.80	99.78	99.75	99.70	99.77	99.78
V	427	378	242	140	218	149	336	300	236	434	195	279
Co	31.1	29.5	21.8	12.2	26.3	20.2	38.1	25.1	27.5	33.2	49.7	53.5
Ga	14.4	16.5	19.6	14.8	14.7	14.2	17.1	15.9	16.7	17.1	14.7	15.8
Rb	22.3	19.7	24.7	91.3	31.2	198.7	3.1	20.4	35.6	17.6	6.3	5.3
Sr	239.7	294.4	441.9	424.5	400.4	209.8	274.1	133.5	401.7	302.0	378.8	342.7
Y	14.4	19.2	23.3	18.1	19.7	23.9	27.0	21.3	23.7	26.4	21.7	25.7
Zr	46.9	61.8	101.0	147.0	97.7	185.4	104.7	175.6	153.5	184.5	76.3	66.2
Nb	4.4	4.5	7.1	9.5	6.7	10.0	25.5	31.5	34.2	38.5	16.0	10.6
Cs	5.0	3.4	8.0	9.0	5.5	22.6	0.4	2.3	5.6	3.9	1.3	0.6
Ba	213	279	426	651	420	534	63	295	442	458	59	85
La	9.7	11.3	18.3	30.7	17.5	31.1	16.0	26.1	27.7	30.6	11.2	5.3
Ce	18.3	22.3	38.1	59.3	36.3	60.6	33.2	48.1	54.3	61.0	23.8	12.7
Pr	2.30	2.98	4.71	6.85	4.47	6.93	4.18	6.16	6.09	7.14	3.00	1.97
Nd	10.1	13.2	18.3	26.2	19.1	26.4	17.6	24.4	23.6	30.7	12.2	8.9
Sm	2.58	3.05	4.49	4.74	4.27	5.16	4.43	4.91	4.97	6.37	3.10	2.66
Eu	0.79	0.95	1.20	1.08	1.13	1.39	1.49	1.59	1.58	1.94	1.01	1.24
Gd	2.84	3.42	4.71	4.10	4.38	5.29	5.01	5.07	4.90	5.92	3.55	3.84
Tb	0.48	0.61	0.66	0.63	0.70	0.85	0.83	0.81	0.73	0.96	0.57	0.71
Dy	2.92	3.61	4.20	3.55	4.00	4.88	5.31	4.59	4.45	5.15	3.79	4.56
Ho	0.61	0.71	0.76	0.75	0.89	1.03	1.13	0.88	0.84	1.10	0.76	0.92
Er	1.75	2.23	2.36	2.18	2.66	3.16	3.52	2.70	2.48	3.25	2.19	2.66
Tm	0.28	0.36	0.32	0.33	0.35	0.46	0.48	0.36	0.34	0.44	0.32	0.36
Yb	1.82	2.39	2.43	2.20	2.50	2.98	2.99	2.47	2.10	3.01	1.92	2.63
Lu	0.28	0.37	0.38	0.33	0.35	0.46	0.47	0.38	0.33	0.42	0.31	0.43
Hf	1.4	1.8	3.5	4.1	2.8	5.0	2.9	3.6	3.5	4.3	1.8	2.3
Ta	0.2	0.3	0.5	0.6	0.4	0.8	1.4	2.0	2.0	2.4	0.9	0.7
Th	2.1	2.5	6.9	19.0	5.3	17.4	3.1	4.4	4.0	5.7	1.3	1.7
U	0.7	1.0	1.6	5.7	1.6	5.6	0.7	0.9	0.9	1.1	0.4	0.3
Eu/Eu*	0.89	0.90	0.79	0.75	0.80	0.81	0.97	0.97	0.97	0.97	0.93	1.19
Mg#	43.7	38.5	52.8	35.2	53.2	39.3	45.9	48.7	59.9	36.4	58.3	55.4

characterized by relative enrichment in Th present in subduction-related basalts plot in the field of volcanic arc basalts (Fig 2c). In the (Th)<sub>N</sub> vs. (Nb)<sub>N</sub> diagram (Saccani, 2015), the samples plot in calc-alkaline basalt, alkali basalt and E-MORB basalt fields (Fig 2d). All these data indicate that the volcanic rocks of the ÇOM can be divided into three groups: 1) enriched mid-ocean ridge basalt (E-MORB)-type, 2) ocean island basalt (OIB)-type and 3) supra-subduction zone (SSZ)-type. The volcanic rocks with OIB affinity contain high TiO<sub>2</sub> (1.64-2.70 wt.%), whereas the E-MORB samples have intermediate TiO<sub>2</sub> (1.10-1.16 wt.%). The SSZ rocks

have low TiO<sub>2</sub> contents ranging from 0.36 to 1.09 wt.%.

In the REE diagram normalized to chondrite, the OIB and E-MORB samples form subparallel patterns, with LREE enrichment compared to the heavy rare earth elements (HREE) (Fig. 3a). The HREE and the LREE concentrations of the OIB rocks are approximately 10 and 100 times higher than those of C1 chondrite, respectively. In the OIB-like samples, (La/Sm)<sub>N</sub> (~ 3.0) and (La/Yb)<sub>N</sub> (~ 6.8) ratios are as high as the average OIB values (Sun and McDonough, 1989). E-MORB-type rocks exhibit flat to slightly enriched LREE patterns ((La/Sm)<sub>N</sub> = 1.26-2.27 and

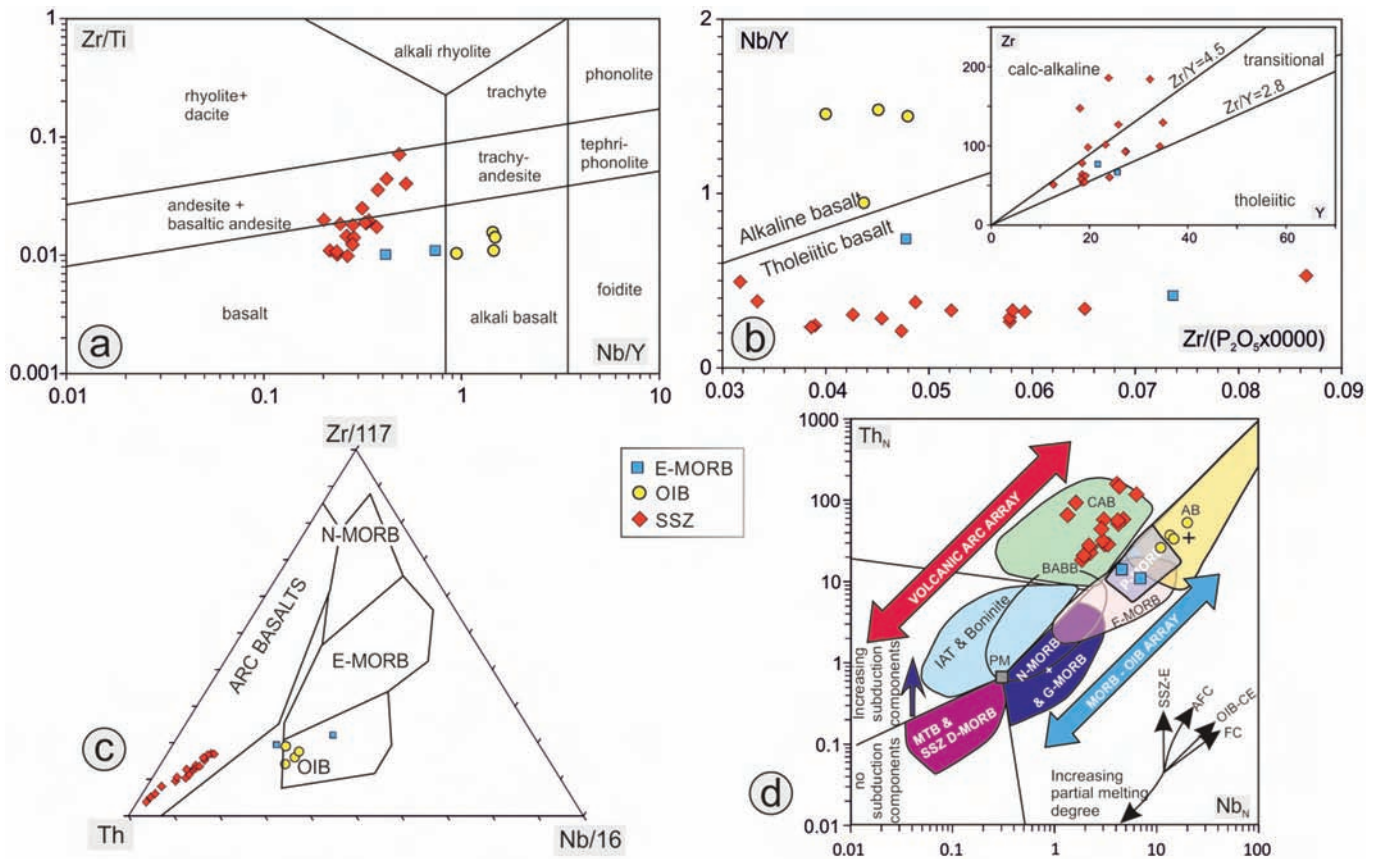


Fig. 2 - a) Zr/Ti versus Nb/Y classification diagram after Pearce (1996); b) Nb/Y vs. Zr/(P<sub>2</sub>O<sub>5</sub> x 10.000) diagram (after Floyd and Winchester, 1975), Inset diagram shows variation of Zr vs. Y for the sub-alkaline volcanic rocks; c) Zr/117-Nb/16-Th diagram showing the basaltic rocks of this study with respect to the fields for ocean island basalt (OIB), volcanic-arc basalt (VAB), normal (N) MORB and enriched (E) MORB (after Wood, 1980); d) Th<sub>N</sub> vs. Nb<sub>N</sub> diagram (Saccani, 2015) showing data of the ÇOM volcanic rocks. Th and Nb are normalized to the N-MORB composition of Sun & McDonough (1989). SSZ-E-supra-subduction zone enrichment; AFC- assimilation-fractional crystallization; OIB-CE- ocean island-type (plume-type) component enrichment; FC- fractional crystallization; MORB- mid-ocean ridge basalt; G-MORB- garnet-influenced MORB; N-MORB- normal-type MORB; E-MORB- enriched-type MORB; P-MORB- plume-type MORB; Ab- alkaline ocean-island basalt; IAT- low-Ti, island arc tholeiite; BON- very low-Ti, boninitic basalt; CAB- calc-alkaline basalt; MTB- medium-Ti basalt; D-MORB- depleted-type MORB; BABB- back arc basin basalt.

(La/Yb)<sub>N</sub> = 1.36-3.93). The SSZ rocks contain partially enriched REE and high LREE concentrations ((La/Sm)<sub>N</sub> = 2.31-4.68 and (La/Yb)<sub>N</sub> = 3.18-10.75). These evolved lavas have almost parallel REE patterns and exhibit 30 to 100 times higher enrichment concentrations with respect to C1 chondrite (Fig. 3b). In addition, the evolved SSZ samples have lower MgO (1.52-5.45 wt.%) and mg-number (Mg-number=100Mg/(Mg/Fe); 31-53). The REE patterns show slightly negative Eu anomalies (Eu/Eu\* = 0.75-0.94) which may be related to plagioclase fractionation.

As a whole, the E-MORB-type samples fall in the range of OIB and E-MORB compositions in the N-MORB-normalized multiple element diagrams (Fig. 3c). These samples are characterized by LREE enrichment and HREE depletion relative to average N-MORB [average (La/Yb)<sub>N</sub> ratios of 2.6]. However, the ratio of Nb/La (1.42-1.97) is higher than average N-MORB (0.83; Saunders and Tarney, 1984), and the Th/Sm ratios (0.41-0.62) are higher than average N-MORB (0.046; Sun and McDonough, 1989). The samples of OIB-type are distinguished by significant enrichment in incompatible elements. Such samples mostly fall between enriched MORB (e.g., E-MORB) and average OIB (Fig 3c). The most important characteristics are positive Nb and Ta anomalies that reflect high Nb/La (1.20-1.59) ratios. High Th/Sm ratios (0.69-0.89) indicate enrichment in the LIL elements.

The SSZ-type rocks show depletion in HFS elements, such as Ta and Nb in MORB-normalized multi-element diagrams (Fig. 3d).

### Sr-Nd-Pb isotopic compositions

The Sr-Nd-Pb isotopic data for the volcanic rocks of the ÇOM are listed in Table 2. While the Sr and Nd isotope ratios in these rocks show a wide range of 0.705776-0.710165 and 0.512507-0.512908, respectively, Pb isotopic data vary in a narrow range. The initial isotopic compositions were recalculated at 100 Ma (early to middle Albian; Beccalotto et al., 2005) according to the greywacke-shale association, the youngest lithology constituting the matrix of mélangé. These sediments are in tectonic contact with basaltic rocks around Çetmibaşıyörükleri in the north of the mélangé (Beccalotto et al., 2005). 100 Ma therefore represents a minimum age correction. However, small changes in the initial ratios do not significantly affect the isotopic signatures of the mantle sources. The initial Sr-Nd isotope ratios are (<sup>87</sup>Sr/<sup>86</sup>Sr)<sub>i</sub> 0.705064 and 0.707060, (<sup>143</sup>Nd/<sup>144</sup>Nd)<sub>i</sub> 0.512633 and 0.512789 for the OIB and E-MORB samples; a relatively broad interval of initial <sup>87</sup>Sr/<sup>86</sup>Sr (0.705350-0.706013) and <sup>143</sup>Nd/<sup>144</sup>Nd (0.512409-0.512681) have been found for the SSZ-type samples. Initial Pb isotopes are (<sup>206</sup>Pb/<sup>204</sup>Pb)<sub>i</sub>

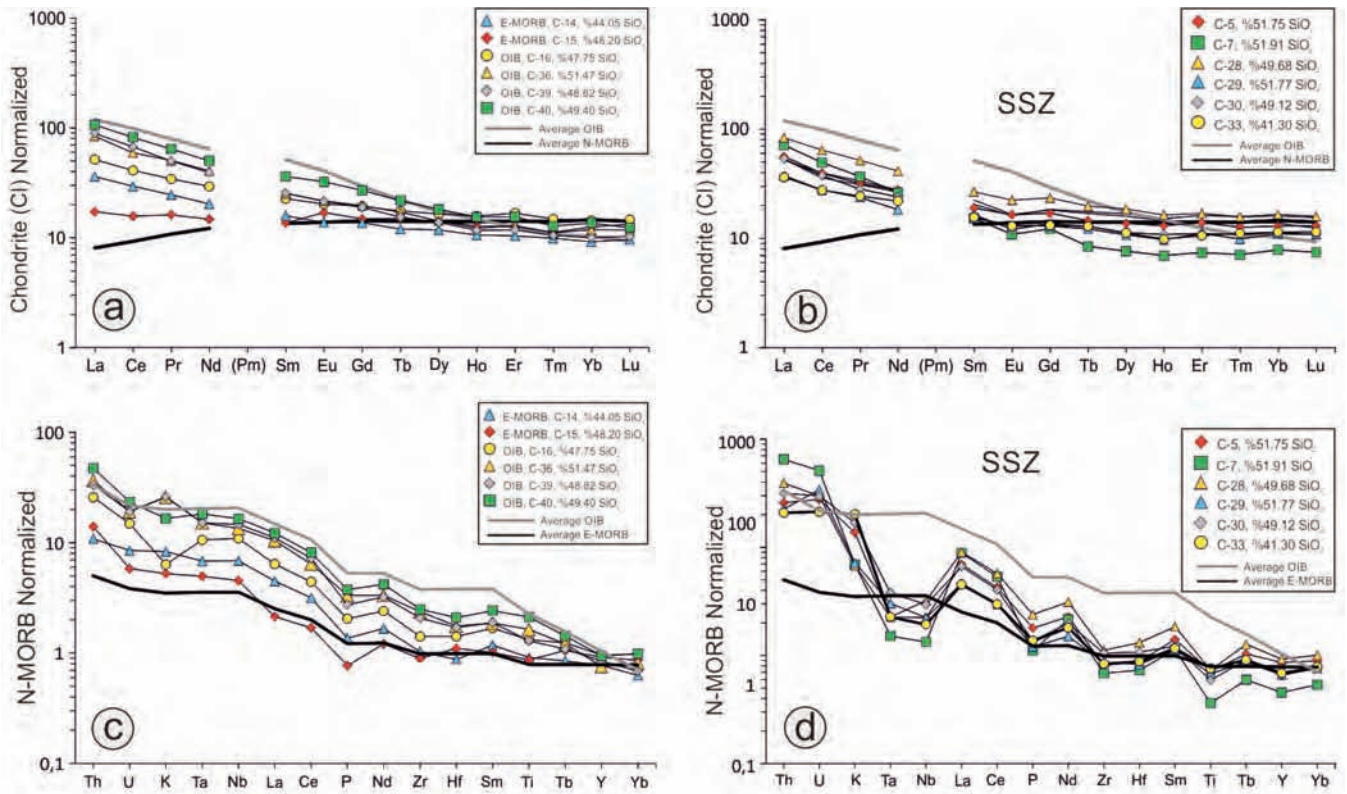


Fig. 3 - Chondrite-normalized REE and N-type MORB normalized multi-element patterns compositions of the ÇOM volcanic rocks. Chondrite normalized REE patterns for a) OIB, E-MORB and b) SSZ. N-MORB normalized multi-element patterns for c) OIB, E-MORB and d) SSZ. Average N-MORB, E-MORB and OIB compositions (Sun and McDonough, 1989) were plotted in the diagrams for comparison. Chondrite normalizing values are from Boynton (1984).

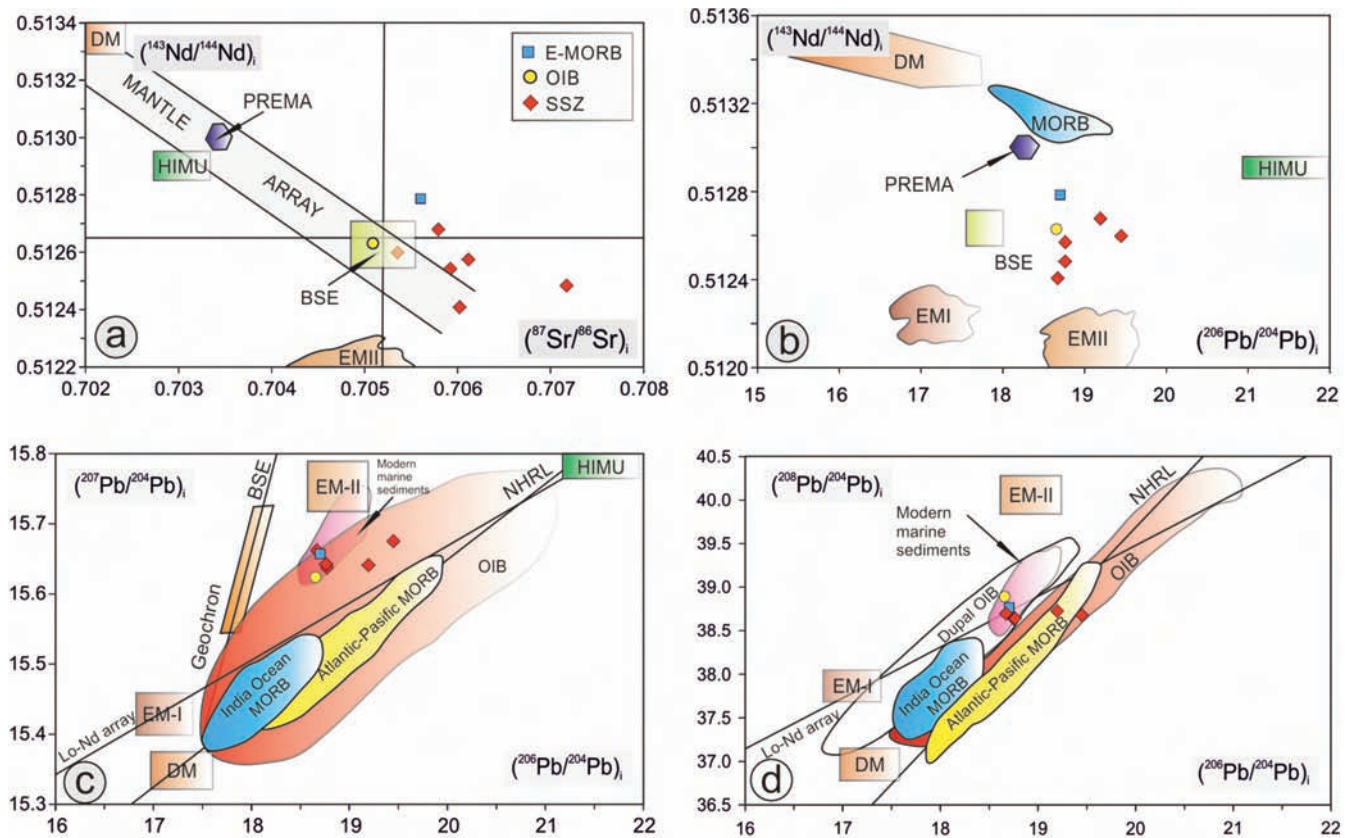


Fig. 4 - a)  $(^{87}\text{Sr}/^{86}\text{Sr})_i$  vs.  $(^{143}\text{Nd}/^{144}\text{Nd})_i$ , b)  $(^{206}\text{Pb}/^{204}\text{Pb})$  vs.  $(^{143}\text{Nd}/^{144}\text{Nd})_i$ , c)  $(^{206}\text{Pb}/^{204}\text{Pb})$  vs.  $(^{207}\text{Pb}/^{204}\text{Pb})$  and d)  $(^{206}\text{Pb}/^{204}\text{Pb})$  vs.  $(^{208}\text{Pb}/^{204}\text{Pb})$  isotope correlation diagrams for the volcanic rocks from the ÇOM. The field of HIMU, OIB, Dupal OIB, EM1 and EM2 are from Hawkesworth et al. (1984), Hart (1984; 1988), Hamelin and Allègre (1985), Hart et al. (1986) and Weaver (1991). The LoNd array and Northern Hemisphere Reference Line (NHRL) are from Hart (1984) and Hart et al. (1986). The fields of Indian Ocean MORB, Atlantic-Pacific MORB and Kerguelen are from Hamelin and Allègre (1985), Barling and Goldstein (1990), Deniel (1998) and references therein.

18.6572 and 18.7031,  $(^{207}\text{Pb}/^{204}\text{Pb})_i$  15.6235 and 15.6564 and  $(^{208}\text{Pb}/^{204}\text{Pb})_i$  38.8787 and 38.7548 for the OIB and E-MORB-type samples, and in the range of  $(^{206}\text{Pb}/^{204}\text{Pb})_i$  18.6715-19.4510,  $(^{207}\text{Pb}/^{204}\text{Pb})_i$  15.6405-15.6749 and  $(^{208}\text{Pb}/^{204}\text{Pb})_i$  38.6231-38.7146 for the SSZ-type samples.

Hydrothermal alteration of the oceanic crust can increase the  $^{87}\text{Sr}/^{86}\text{Sr}$  ratios of oceanic rocks (McCulloch et al., 1981, Godard et al., 2006), whereas Nd is relatively immobile in fluids (Faure and Mensing, 2004) if the water/rock ratio with alteration does not exceed  $10^5$ . For this reason, we conclude that the  $^{143}\text{Nd}/^{144}\text{Nd}$  ratios of the samples were not significantly changed by seawater alteration. On the other hand, as U and Pb are mobile during hydrothermal alteration processes, the Pb isotopic composition may be affected (Faure and Mensing, 2004); in particular, the addition of U may increase the ratio of  $^{206}\text{Pb}/^{204}\text{Pb}$  over time. Th is relatively immobile and the low abundance of  $^{235}\text{U}$ ,  $^{207}\text{Pb}/^{204}\text{Pb}$  and  $^{208}\text{Pb}/^{204}\text{Pb}$  ratios reflect the isotopic composition of the mantle source (Hauff et al., 2003; Liu et al., 2013).

For comparison, Sr-Nd diagram shows the fields for common isotopic reservoir (Fig. 4a). In the  $^{143}\text{Nd}/^{144}\text{Nd}$  versus  $^{87}\text{Sr}/^{86}\text{Sr}$  correlation plot, the volcanic rocks of the Çetmi

Ophiolitic Mélange have distinctly different Nd isotopic compositions. The range of Nd isotopes can explain mixed mantle components in the source region. The highest Sr isotope ratios are shown by one sample (sample C-21). These high Sr isotope ratios may reflect the addition of Sr from seawater during post-magmatic alteration or the addition of radiogenic Sr to the source of the primary mantle by fluids derived from the dehydrating slab. In the  $(^{143}\text{Nd}/^{144}\text{Nd})_i$  vs  $(^{206}\text{Pb}/^{204}\text{Pb})_i$  diagram, the isotopic ratios of the samples cluster between the Bulk Silica Earth (BSE) and MORB fields indicating that the samples may derived from enriched source (Fig. 4b).

In the  $(^{207}\text{Pb}/^{204}\text{Pb})_i$ - $(^{206}\text{Pb}/^{204}\text{Pb})_i$  isotope diagram, the volcanic rocks of this study plot at the right of the geochron, above the NHRL and LoNd array (Fig. 4c; Hart, 1984; Hart et al., 1986); a broad trend towards EMII reference reservoir can be also observed. In the correlation diagrams of  $(^{208}\text{Pb}/^{204}\text{Pb})_i$  vs  $(^{206}\text{Pb}/^{204}\text{Pb})_i$  the rock samples plot above the OIB and MORBs field, which imply derivation from a MORB mantle source and the possible involvement of modern marine sediments (Fig 4d). The trend toward the sediments in the diagram is an important characteristic of the island arc and some back arc volcanism.

Table 2- Sr, Nd and Pb isotopic compositions of the volcanic rocks from the ÇOM.

Sample	C-1	C-4	C-21	C-28	C-32	C-34	C-36	C-15
Mag. affinity	SSZ	SSZ	SSZ	SSZ	SSZ	SSZ	OIB	E-MORB
Sr	141.56	319.78	125.43	167.44	279.15	441.94	150.31	342.67
Rb	15.97	13.59	94.71	18.68	25.60	24.71	26.04	5.30
Sm	5.27	4.59	6.05	5.21	2.67	4.49	7.04	2.66
Nd	22.75	23.09	30.50	24.80	11.65	18.27	30.07	8.86
Th	6.90	11.11	14.01	6.70	3.31	6.88	6.20	1.68
U	1.21	0.42	3.43	1.60	0.75	1.58	1.10	0.27
Pb	4.80	6.46	18.08	7.40	2.48	11.13	5.75	10.45
$^{87}\text{Sr}/^{86}\text{Sr}$	0.706566	0.705525	0.710165	0.706365	0.706156	0.706243	0.705776	0.705664
Error 2 $\sigma$	0.000010	0.000013	0.000005	0.000005	0.000011	0.000010	0.000014	0.000017
$^{87}\text{Rb}/^{86}\text{Sr}$	0.326455	0.122922	2.185338	0.322674	0.265297	0.161774	0.501176	0.044770
$(^{87}\text{Sr}/^{86}\text{Sr})_i$	0.706119	0.705357	0.707171	0.705923	0.705792	0.706021	0.705089	0.705603
$^{143}\text{Nd}/^{144}\text{Nd}$	0.512668	0.512680	0.512564	0.512627	0.512772	0.512507	0.512726	0.512908
Error 2 $\sigma$	0.000002	0.000002	0.000002	0.000002	0.000005	0.000003	0.000002	0.000003
$^{147}\text{Sm}/^{144}\text{Nd}$	0.140603	0.120822	0.120462	0.127555	0.139104	0.149151	0.142278	0.182532
$(^{143}\text{Nd}/^{144}\text{Nd})_i$	0.512576	0.512601	0.512485	0.512544	0.512681	0.512409	0.512633	0.512789
$\epsilon\text{Nd}_{(100)}$	1.30	1.79	-0.47	0.67	3.35	-1.95	2.41	5.45
$^{208}\text{Pb}/^{204}\text{Pb}$	39.0707	39.2044	38.8699	-	39.1297	38.8748	39.2142	38.8048
Error 2 $\sigma$	0.0023	0.0049	0.0046	-	0.0100	0.0062	0.0039	0.0071
$^{207}\text{Pb}/^{204}\text{Pb}$	15.6568	15.6779	15.6505	-	15.6544	15.6682	15.6323	15.6576
Error 2 $\sigma$	0.0008	0.0020	0.0016	-	0.0034	0.0022	0.0015	0.0023
$^{206}\text{Pb}/^{204}\text{Pb}$	19.0096	19.5127	18.9445	-	19.4816	18.8063	18.8381	18.7280
Error 2 $\sigma$	0.0007	0.0024	0.0014	-	0.0030	0.0020	0.0015	0.0020
$^{232}\text{Th}/^{204}\text{Pb}$	90.2575	108.0405	48.6667	-	83.7001	38.7797	67.6615	10.0801
$^{235}\text{U}/^{204}\text{Pb}$	0.1125	0.0290	0.0848	-	0.1341	0.0633	0.0850	0.0117
$^{238}\text{U}/^{204}\text{Pb}$	15.3155	3.9440	11.5186	-	18.2497	8.6220	11.5681	1.5924
$(^{208}\text{Pb}/^{204}\text{Pb})_i$	38.6231	38.6685	38.6285	-	38.7146	38.6825	38.8787	38.7548
$(^{207}\text{Pb}/^{204}\text{Pb})_i$	15.6452	15.6749	15.6418	-	15.6405	15.6617	15.6235	15.6564
$(^{206}\text{Pb}/^{204}\text{Pb})_i$	18.7701	19.4510	18.7644	-	19.1963	18.6715	18.6572	18.7031

### Source characteristics of the volcanic rocks

The geochemical characteristics described above indicate that volcanic rocks of the Çetmi Mélange have OIB, E-MORB and SSZ-signatures. Isotopic compositions of some of the samples plot close to the MORB field and within OIB field (Fig. 4). In order to determine the source characteristics of the volcanic rocks, such as E-MORB and OIB, highly incompatible to moderately incompatible element ratios (La/Sm vs. La and La/Yb vs. Zr/Nb, e.g., Aldanmaz, et al., 2000; Aldanmaz et al., 2006) were used (Fig. 5a, b). According to the diagrams based on these ratios, the E-MORB and OIB-type samples have higher La/Yb and lower Zr/Nb ratios than those that can be produced by single stage partial melting from common mantle sources such as DMM and PM. It also indicates that the OIB samples may be generated with a low-degree partial melting (~ 5-8%) of the enriched source. Some OIB samples of the Çetmi Mélange plot close to the mantle array and follow the melting curve drawn for spinel-lherzolite mantle source. One sample with E-MORB composition is the result of a mixing between enriched and depleted mantle source. On the other hand, slightly negative  $\Delta Hf$  for the OIB and E-MORB samples (Fig. 5d) and the depletion of Zr and Hf (Fig. 3c) relative to Nd indicate the involvement of subduction-derived aqueous fluids. Such trace element characteristics of the E-MORB-OIB-type samples show that they can occur in the vicinity of subduction. Percolation and differentiation of a melt produced by a low degree partial melting of a MORB mantle or of a slight-

ly enriched mantle source may create metasomatic veins as a potential source for OIB (Pilet et al., 2005). In these samples, Pb isotope compositions towards the EMII (Fig. 4c, d) indicate the differentiation by long-term Pb evolution in the generation of the mantle reservoir (Seal et al., 1998). This process, which generates different vein compositions within the lithosphere, leads to a decrease in U/Pb, Th/Pb and an increase of Pb from the bottom to top of oceanic lithosphere prior to subduction (Pilet et al., 2005). The continuous change of U/Pb and Th/Pb from the bottom to the top of the lithosphere causes a decrease in  $^{206}\text{Pb}/^{204}\text{Pb}$  in relation to an increase in  $^{207}\text{Pb}/^{206}$  and  $^{208}\text{Pb}/^{206}\text{Pb}$  after the sufficient isolation period. Pilet et al. (2005) suggested that EMII end member isotopic and chemical compositions are produced by the trace element fractionation and the metasomatic processes in the lithosphere. For these samples, the Nb-Ta peaks can be explained by the presence of amphibole in the source, possibly occurring in veins. Melting of amphibole-bearing veins, which have lower solidus temperature than peridotite in the metasomatized lithospheric mantle, may cause Nb-Ta peaks in the OIB-type samples. During the magma ascent, these melts can produce enriched MORB magmas due to mixing with the depleted mantle melts (e.g., Wong, et al., 2010).

The SSZ-type samples are characterized by LREE enrichment and HFSE depletion, such as Nb-Ta negative anomalies (Fig. 3d), indicating interaction with slab-derived fluids into the mantle source. The SSZ volcanics show a slight calc-alkaline affinity with Ta, Nb and Ti depletion.

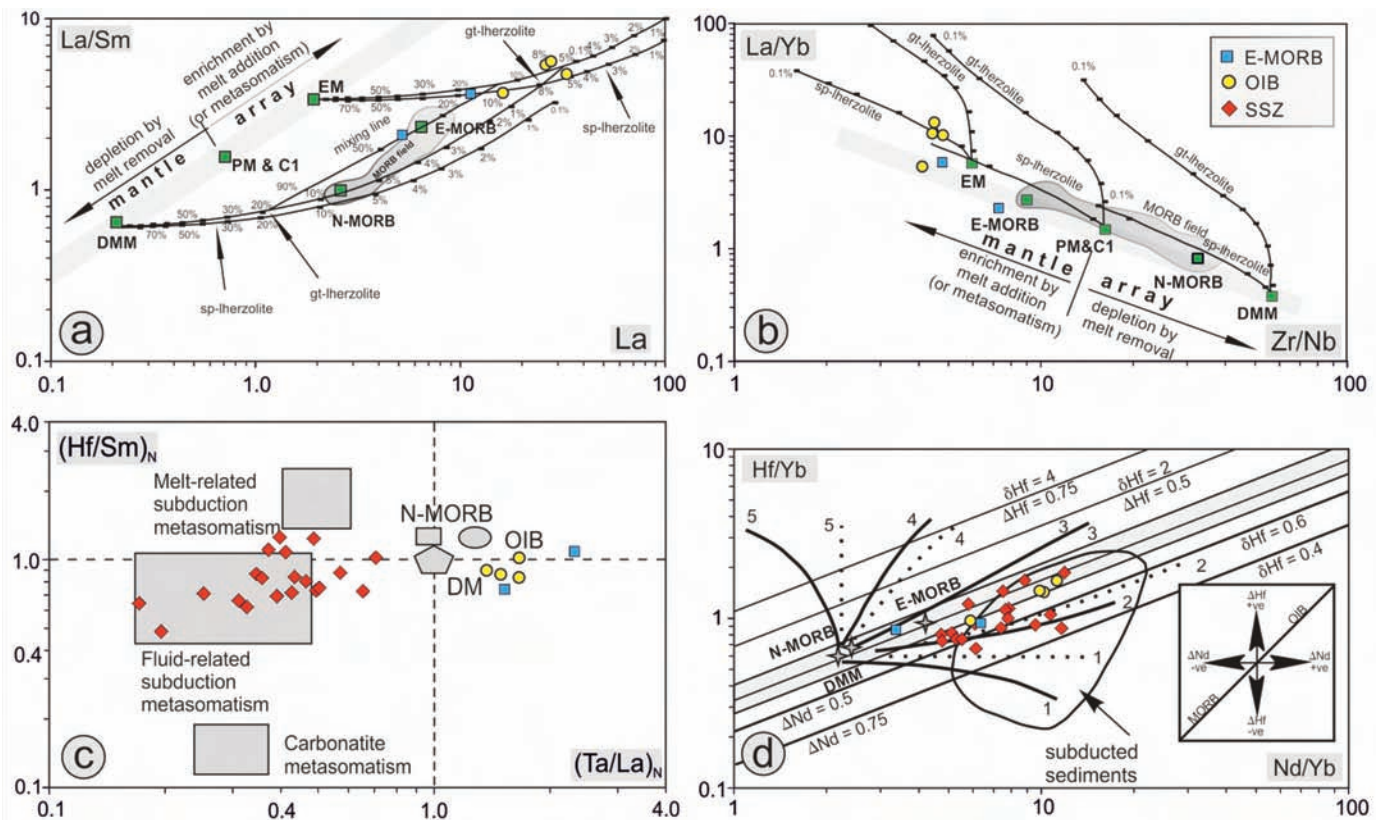


Fig. 5 - a) Plot of La vs. La/Sm; b) Plot of La/Yb vs. Zr/Nb (after Aldanmaz et al., 2008; melt curves obtained for non-modal batch melting model by Aldanmaz et al., 2006). Numbers on curves indicate degree of partial melting. DM, depleted mantle; PM, primitive mantle; EM, enriched mantle. c)  $(\text{Hf}/\text{Sm})_N$  vs.  $(\text{Ta}/\text{La})_N$  diagram (LaFlèche et al., 1998). Normalization values are from Sun and McDonough (1989). d) Nd/Yb-Hf/Yb variation diagram (after Pearce et al., 1999). The curves are mixing trends between DM (depleted mantle) and subducted pelagic sediment modeled with a mass fraction from 0.05 to 0.2 of subduction component in the mantle. Ratios for Hf and Nd between subduction component and mantle are represented by  $r\text{Hf}$  and  $r\text{Nd}$ . (Please refer to the reference paper for definitions and modeling method).

This may imply that the mantle source was depleted by previous melt extraction events (Pearce, 1982). The depletion of Ta and Hf relative to La and Sm, respectively, is thought to be the result of fluid-related metasomatism through subduction. These rocks have  $(\text{Ta/La})_N$  ratios ranging from 0.17 to 0.65 and  $(\text{Hf/Sm})_N$  ratios ranging from 0.48 to 1.45, plotting along the trajectory between MORB and metasomatized components in  $(\text{Ta/La})_N$  and  $(\text{Hf/Sm})_N$  diagrams (Fig. 5c; e.g., La Flèche et al., 1998).

Alternatively, Hf-Nd trace element systems can be used to constrain the involvement of subduction-derived material. Although HFSE and REE generally behave similarly during partial melting of MORB and OIB mantle source, the HFSE anomalies are due to different behaviour of these groups of elements in subduction systems (e.g., Thirlwall et al., 1994; Pearce and Peate, 1995). Both fluids released from the slab during dehydration or silicate melts generated by partial melting of the slab components can be considered as slab-derived components. Since Nd is generally more soluble in siliceous melts and aqueous fluids than Hf, Hf-Nd variations can provide constraints on the origin of the subduction component. Therefore, Hf cannot be easily transported to the mantle wedge by slab dehydrated fluids (e.g., Barry et al., 2006). In the Nd/Yb vs Hf/Yb diagram proposed by Pearce et al. (1999), the displacement from the mantle trend showing the average MORB-OIB composition (shaded area) is denoted by  $\Delta\text{Hf}$  (+ and Hf anomaly) and  $\Delta\text{Nd}$  (- and Hf anomaly) (Fig. 5d).  $\Delta\text{Hf}$  and  $\Delta\text{Nd}$  thus define the extent of the positive and negative displacements of the samples. Most of the SSZ samples from the ÇOM show negative  $\Delta\text{Hf}$  trends. The negative  $\Delta\text{Hf}$  anomalies indicate that SSZ volcanics are the product of a depleted MORB mantle that interacted with subduction fluids due to slab dehydration. However, slightly positive and negative  $\Delta\text{Hf}$  anomalies are observed in some samples. The enrichment of Hf relative to the REE may be explained by fractional crystallization of low-Mg amphibole (Pearce et al., 1999). These magmas were likely originated from mantle wedge metasomatized by the slab-derived material, since the formation of low-Mg amphibole may be facilitated by infiltration of silica rich aqueous fluids or water-rich silicic melt (Ionov and Hofmann, 1995; Laurora et al., 2001). In addition, most of the SSZ-type lavas have relatively low  $\epsilon\text{Nd}(i)$  values and radiogenic Pb isotope ratios close to a MORB source that is contaminated by subduction-related components. As a whole, the Sr-Nd-Pb isotope compositions point to the involvement of crustal (sedimentary) components (Fig. 4).

## GEODYNAMIC IMPLICATIONS

Ophiolites are formed in oceanic spreading ridges, hot spots, and suprasubduction zone (SSZ) environments, such as intra-oceanic arcs, continental arcs, forearcs, and back-arcs (e.g., Pearce, 2008; Dilek and Furnes, 2011; Saccani, 2015). Magmatic rocks in ophiolites provide valuable information about crustal accretion processes in different tectono-magmatic environments. The scattered outcrops of the ÇOM on the Biga and Gelibolu Peninsula are interpreted as remnants of the Intra-Pontide suture between the Sakarya terrane in the southeast and the Rhodope domain in the northwest of the region (Siyako et al., 1989; Okay and Tüysüz, 1999; Beccalotto et al., 2005). In addition, the Çetmi Mélange in the Biga Peninsula may represent the westernmost outcrops of the IPS, as firstly suggested by

Göncüoğlu et al. (1997). This suture formed as a result of the northward subduction of the Intra-Pontide Ocean during the Cretaceous (Bergougnan, 1975; Koçyigit, 1991; Okay and Şahintürk, 1997; Okay and Tüysüz, 1999). During the collision between the Rhodope-Istranca Massif and the Ezine-Sakarya terrane in the Late Paleocene, the accretionary prism represented by the ÇOM was pushed south-east and tectonically covered a part of the Ezine and Sakarya terranes. The youngest lithology of the mélange is the early to middle Albian greywacke-shale association matrix (Beccalotto, et al., 2005). The lack of radiometric ages for the different types of volcanic rocks occurring as tectonic slices in the mélange, prevents to assess the temporal geochemical variations of the magmatic events that occur throughout the whole history of the ophiolite formation. However, it is possible to identify the mantle source characteristics and the geodynamic setting responsible for the formation of the oceanic crust fragments found in the mélange.

The geochemical signatures of the magmatic rocks in the ophiolites can give information about the tectonic setting of the primary magma source. In the Y vs. La/Nb (Fig. 6a, Floyd et al., 1991), Zr vs. V/Ti (Fig. 6b, Woodhead et al., 1993), Zr vs. Zr/Y (Fig. 6c, Pearce and Norry, 1979) and V vs. Ti/1000 (Fig. 6d, Shervais, 1982) tectonic discrimination diagrams, the basaltic rock samples from the ÇOM fall in the MORB, back-arc basin basalt (BABB) and island arc basalt (IAB) fields (Fig. 6). The different geochemical characteristics of the basaltic rocks in the mélange indicate that the oceanic crust formation occurs in more than one stage. Although subduction-related affinity rocks dominate in back-arc basins, MORB and OIB-type extrusive rocks may also occur in back-arc basins (e.g., Saunders and Tarney 1984; Aldanmaz et al., 2008). Such MORB/OIB to island arc geochemical features with source heterogeneity are the characteristic of the ophiolites formed in back-arc basins (e.g., Pearce et al., 1984; Gribble et al., 1998; Sinton et al., 2003). The dominant BABB type rocks showing some E-MORB and OIB-like affinity reflect back-arc environments (Pearce et al., 1994), while spreading axis close to the arc-trench system are characterized by the transition between the N-MORB and IAB signatures. In addition, the compositional diversity of the back-arc basin lavas is explained by the source heterogeneity which indicates a variable mixing of fertile mantle, depleted mantle and slab-derived components (Taylor and Martinez, 2003; Kuzmichev et al., 2005).

In an island arc-back-arc system, magmatic activity occurs both along island arc and the spreading centre of the BAB. The BAB rifting begins at a region close to the axis of magmatic arc and gradually moves away from the subduction zone and the axis along with the spread of the BAB (Taylor and Martinez, 2003). Thus, depending on the stage of development of the BAB, the geochemical characteristics varying from the IAB to MORB are determined by the interaction between the mantle and the subduction zone components (e.g., Stern et al., 1990). According to Pearce (2008), the back-arc basalts have MORB (OIB) affinity if the source region is not affected by the subduction components; however, deviation from typical MORB-OIB compositions increases with increasing involvement of subduction-related components.

The occurrence of MORB-OIB rocks in the Çetmi Mélange indicates interaction of two different sources characterized by a mixture of enriched and depleted mantle domains. Eruption of enriched OIB-type rocks is not only limited to intraplate plume-related settings but they can be

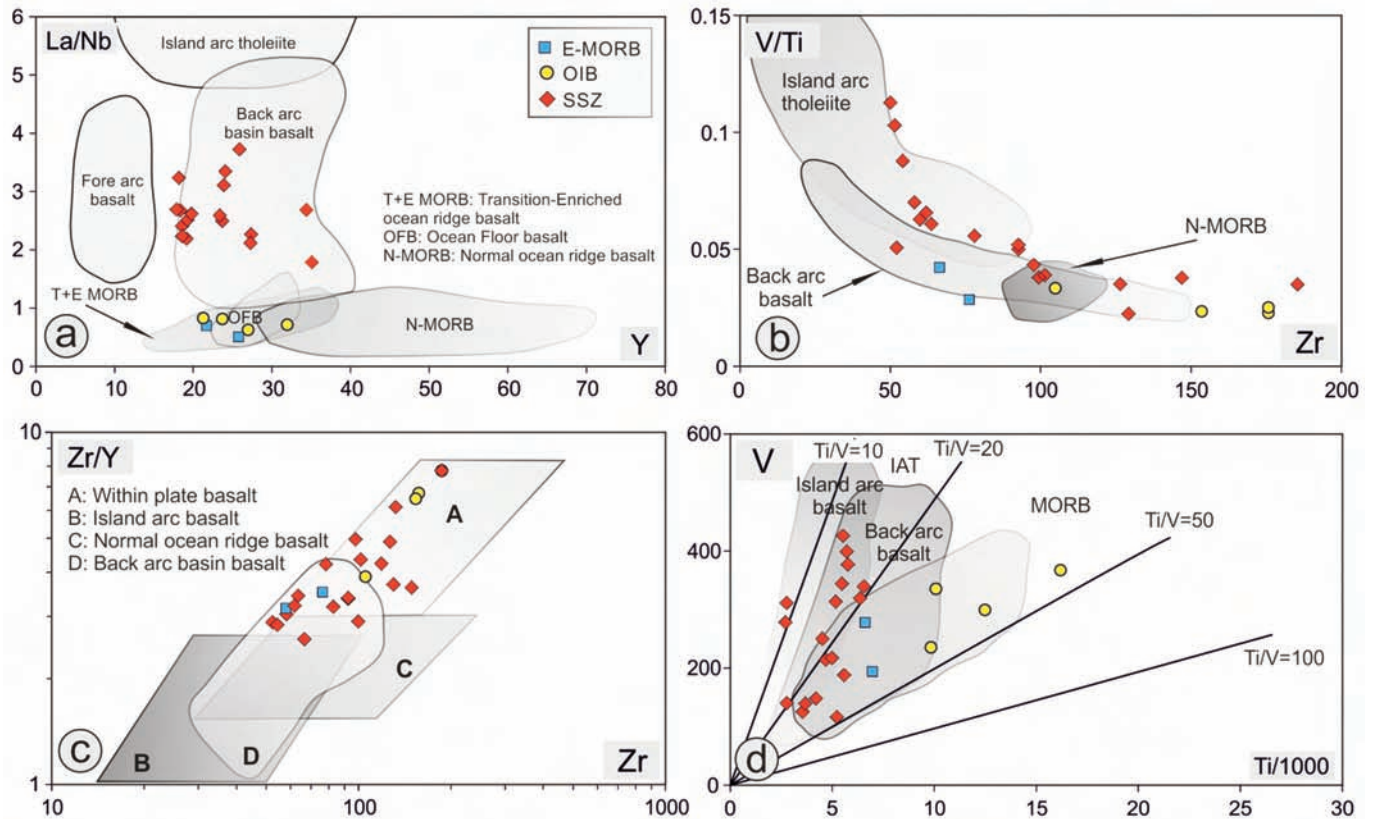


Fig. 6 - Tectonic discrimination diagrams for the volcanic rocks from the ÇOM. a) La/Nb vs. Y (Floyd et al., 1991); b) Zr vs. V/Ti (Woodhead et al., 1993); c) Zr vs. Zr/Y (Pearce and Norry, 1979; revised from Floyd et al., 1991); d) V vs. Ti/1000 (Shervais, 1982) plots.

found also in both fast- and slow-spreading ridges (Niu et al., 1999; Hemond et al., 2006; Nauret et al., 2006). Metasomatic amphibole-bearing veins can be produced within the oceanic lithosphere by infiltration of low-degree melts. Geochemical characteristics of E-MORB and OIB-type samples may be explained by decompression melting of previously-metasomatized ancient lithospheric blocks in a back-arc spreading centre.

In SSZ-type volcanic rocks, relative depletion in HFSE elements (such as Nb-Ta) and enrichment in Th compared to N-MORB are usually observed, indicating a subduction-modified upper mantle source. The LILE/HFSE and HFSE/LFSE ratios in the SSZ samples with slight calc-alkaline affinity are very similar to those observed in modern intra-oceanic arcs (e.g., Middle Jurassic ophiolites in the South Apuseni Mountains; Nicolae and Saccani, 2003). The high Th and LREE contents and highly radiogenic Pb isotopic composition of the samples compared to MORB are similar to the trace element and isotope values of the global pelagic sediments. Such high Pb isotopic ratios and high Th and LREE trace element characteristics indicate the contribution of subducted sediments to the mantle source. SSZ-type volcanic rocks with arc affinity are derived by interaction between MORB-like mantle in the extensional back-arc setting and the subduction components (Stern et al., 1990; Gribble et al., 1996; Pearce and Stern, 2006). For this reason, SSZ-type volcanic rocks are thought to have been produced by the melting of a depleted mantle source contaminated by the hydrothermal slab-derived fluids in a back-arc basin environment.

The westernmost outcrops of the IPS zone are represented by the ÇOM on the Biga Peninsula; however, in the north-

western and central Turkey, the IPS zone is characterized by several bodies of ophiolite-bearing mélanges that crop out from the Armutlu Peninsula to the Araç Area (Göncüoğlu et al., 2014). This zone also consists of a west-east-trending oceanic domain that extended from the Balkans to the central Anatolia (Marroni et al., 2014). While several researchers have suggested that the Izmir-Ankara-Erzincan Suture Zone represents the eastern extension of the Balkan ophiolites, Bortolotti et al. (2013) suggest a very similar geodynamic evolution of the Intra-Pontide and the Vardar Oceanic Basin. Although characterized by the occurrence of CAB, BABB and N-MORBs, similar examples of continental arc-back-arc settings are common in the Mesozoic peri-Mediterranean Tethys, particularly in the Vardar zone (e.g., Bortolotti et al., 2002; Nicolae and Saccani, 2003; Saccani et al., 2008; Schmid et al., 2008; Hoeck et al., 2009; Ionescu et al., 2009). According to the geochemical characteristics of the volcanic rocks of the ÇOM, closure of the Intra-Pontide Ocean in the western Anatolia was related to an intra-oceanic subduction generating an arc-basin system.

## CONCLUSIONS

The major, trace element and Sr-Nd-Pb isotopic characteristics of the volcanic rocks of the ÇOM indicate OIB, E-MORB and SSZ-type formations. In the OIB type rocks, the depletion in Zr and Hf relative to Nd and the slightly negative  $\Delta Hf$  show the effect of slab-derived fluids in the source regions. The E-MORB affinity samples indicate a mixing of enriched and depleted sources, while the OIB samples are produced by lower degrees of melting of an enriched source.

In the OIB type rocks, the Nb-Ta positive anomalies suggest a source characterized by the presence of amphibole in enriched domains due to the metasomatic processes in the oceanic lithospheric mantle. The high Pb isotope ratios shifted towards EMII in OIB and E-MORB samples are consistent with metasomatic processes in the oceanic lithosphere. The SSZ-type samples, which constitute most of the samples in the mélange, are characterized by enrichment in LREE and depletion in HFSE such as Nb-Ta negative anomalies, possibly indicating the involvement of slab-derived fluids instead of melts derived from oceanic crust and/or sediments. High LILE and depletion in HFSE as well as Sr-Nd-Pb isotopic signatures of the SSZ-type volcanic rocks indicate derivation of the magmas from a depleted MORB-type mantle contaminated by subducted components. Source heterogeneity related to variable mixing of mantle source indicates that the volcanic rocks of the ÇOM which is well represent the westernmost outcrop of Intra Pontide Suture in Biga Peninsula were generated in a arc-basin system.

### ACKNOWLEDGEMENTS

This research was financially supported by the Research Fund of Kocaeli University (Project No: 2015/19). The author thanks Dr. Ercan Aldanmaz for his valuable contributions to this work and M.C. Göncüoğlu (METU) and E. Saccani (Ferrara) for their constructive reviews.

### REFERENCES

- Akbayram K., Okay A.I. and Satır M., 2012. Early Cretaceous closure of the Intra-Pontide Ocean in western Pontides (northwestern Turkey). *J. Geodyn.*, 65: 38-55.
- Aldanmaz E., Köprübaşı N., Gürer Ö. F., Kaymakçı N. and Gourgaud A., 2006. Geochemical constraints on the Cenozoic, OIB-type alkaline volcanic rocks of NW Turkey. Implications for mantle sources and melting processes. *Lithos*, 86: 50-76.
- Aldanmaz E., Pearce J.A., Thirlwall M.F. and Mitchell J.G., 2000. Petrogenetic evolution of Late Cenozoic, post-collision volcanism in western Anatolia, Turkey. *J. Volcan. Geoth. Res.*, 102: 67-95.
- Aldanmaz E., Yalınız M.K., Güçtekin A. and Göncüoğlu M.C., 2008. Geochemical characteristics of mafic lavas from the Neotethyan ophiolites in western Turkey: implications for heterogeneous source contribution during variable stages of ocean crust generation. *Geol. Mag.*, 145: 37-54.
- Aygül M., Topuz, G., Okay A.I., Satır M. and Meyer H.P., 2012. The Kemer Metamorphic Complex (NW Turkey), a subducted continental margin of Sakarya Zone: *Turk. J. Earth Sci.*, 21 (1): 19-35.
- Bailey E.B. and McCallien W.J., 1950. The Ankara Mélange and the Anatolian Thrust. *Nature*, 166: 938-940.
- Barling J. and Goldstein S.L., 1990. Extreme isotopic variations in Heard Island lavas and the nature of mantle reservoirs. *Nature*, 348: 59-62.
- Barry T.L., Pearce J.A., Leat P.T., Millar I.L. and le Roex A.P., 2006. Hf isotope evidence for selective mobility of high-field-strength elements in a subduction setting: South Sandwich Islands. *Earth Planet. Sci. Lett.*, 252: 223-244.
- Beccalotto L., 2003. Geology, correlations, and geodynamic evolution of the Biga Peninsula (NW Turkey). PhD Thesis, Univ. Lausanne, Switzerland [unpublished].
- Beccalotto L., Bartolini A.C., Martini R., Hochuli P. and Kozur H., 2005. Biostratigraphic data from the Çetmi mélange, northwest Turkey: palaeogeographic and tectonic implications. *Palaeo., Palaeo.*, 221: 215-244.
- Bergougnan H., 1975. Relations entre les édifices pontiques et taurique dans le nord-est de l'Anatolie. *Bull. Soc. Géol. Fr.*, 17: 1045-1057.
- Bingöl E., Akyürek B. and Korkmaz B., 1975. Geology of the Biga Peninsula and some characteristic of the Karakaya blocky series. *Proceed. Congr. Earth Sci.*, 50<sup>th</sup> Anniversary of the Republic Turkey. *Min. Res. Explor. Inst.*, Ankara, p. 70-76 (in Turkish).
- Bortolotti V., Chiari M., Göncüoğlu M.C., Marcucci M., Principi G., Tekin U.K., Saccani E. and Tassinari R., 2013. Age and geochemistry of basalt-chert associations in the ophiolitic complexes of the Izmir-Ankara Mélange East of Ankara, Turkey: preliminary data. *Ophiolite*, 38:157-173.
- Bortolotti V., Marroni M., Nicolae I., Pandolfi L., Principi G. and Saccani E., 2002. Geodynamic implications of Jurassic ophiolites associated with island-arc volcanics, South Apuseni Mountains, western Romania. *Intern. Geol. Rev.*, 44: 938-955.
- Boynton W.V., 1984. Geochemistry of the rare earth elements: meteorite studies. In: P. Henderson (Ed.), *Rare earth element geochemistry*. Elsevier, p. 63-114.
- Deniel C., 1998. Geochemical and isotopic (Sr, Nd, Pb) evidence for plume-lithosphere interactions in the genesis of Grande Comore magmas (Indian Ocean). *Chem. Geol.*, 144: 281-303.
- Dewey J.F. and Bird J.M., 1971. Origin and emplacement of the ophiolite suite: Appalachian ophiolites in Newfoundland. *J. Geophys. Res.*, 76 (14): 3179-3203.
- Dilek Y. and Flower M.F.J., 2003. Arc-trench rollback and forearc accretion: 2. Model template for Albania, Cyprus, and Oman. In: Y. Dilek and P.T. Robinson (Ed.), *Ophiolites in Earth History*. *Geol. Soc. London Spec. Publ.*, 218: 43-68.
- Dilek Y. and Furnes H., 2011. Ophiolite genesis and global tectonics: geochemical and tectonic fingerprinting of ancient oceanic lithosphere. *Geol. Soc. Am. Bull.*, 123: 387-411.
- Dilek Y. and Furnes H., 2014. Ophiolites and their origins: *Elements*, 10: 93-100, doi: 10.2113/gselements.10.2.93.
- Elmas A., Yiğitbaş E. and Yılmaz Y., 1997. The geology of the Bolu-Eskipazar zone: an approach to the development of the Intra-Pontide Suture. *Geosound*, 30: 1-14.
- Ercan T., Satır M., Steinitz G., Dora A., Sarıfakıoğlu E., Adis C., Walter H.J. and Yıldırım T., 1995. Biga Yarımadası ile Gökçeada, Bozcaada ve Tavşan adalarındaki (KB Anadolu) Tersiyer volkanizmasının özellikleri. *MTA Dergisi*, 117: 55-86 (in Turkish).
- Faure G. and Mensing T.M., 2004. *Isotopes: Principles and applications*, 3<sup>rd</sup> ed. John Wiley and Sons Press, 897 pp.
- Floyd P.A. and Winchester J.A., 1975. Magma-type and tectonic setting discrimination using immobile elements. *Earth Planet. Sci. Lett.*, 27: 211-218.
- Floyd P.A. and Winchester J.A., 1978. Identification and discrimination of altered and metamorphosed volcanic rocks using immobile elements. *Chem. Geol.*, 21: 291-306.
- Floyd P.A., Kelling G., Gökçen S.L. and Gökçen N., 1991. Geochemistry and tectonic environment of basaltic rocks from the Misis ophiolitic mélange, South Turkey. *Chem. Geol.*, 89: 263-280.
- Gribble R.F., Stern R.J., Bloomer S.H., Stuben D., O'Hearn T. and Newman S., 1996. MORB mantle and subduction components interact to generate basalts in the southern Mariana through back-arc basin. *Geochim. Cosmochim. Acta*, 60: 2153-2166.
- Gribble R.F., Stern R.J., Newman S., Bloomer S.H. and O'Hearn T., 1998. Chemical and isotopic composition of lavas from the Northern Mariana Trough: implications for magmagenesis in back-arc basins. *J. Petrol.*, 39: 125-154.
- Godard M., Bosch D. and Einaudi F., 2006. A MORB source for low-Ti magmatism in the Semail ophiolite. *Chem. Geol.*, 234: 58-78.
- Göncüoğlu M.C. and Erendil M., 1990. Pre-Late Cretaceous tectonic units of the Armutlu Peninsula. *Proceed. 8<sup>th</sup> Turkish Petrology Congr.*, 8: 161-168.
- Göncüoğlu M.C., Dirik K. and Kozlu H., 1997. General characteristics of pre-Alpine and Alpine terranes in Turkey: explanatory notes to the terrane map of Turkey. *Ann. Géol. Pays Hellén.*, 37: 515-536.

- Göncüoğlu M.C., Gürsu S., Tekin U.K., Köksal S., 2008. New data on the evolution of the Neotethyan oceanic branches in Turkey: late Jurassic ridge spreading in the Intra-Pontide branch. *Ofioliti*, 33: 153-164.
- Göncüoğlu M.C., Marroni M., Pandolfi L., Ellero A., Ottria G., Catanzariti R., Kagan U.T. and Sayit, K., 2014. The Arkot Dağ Mélange in Araç area, central Turkey: Evidence of its origin within the geodynamic evolution of the Intra-Pontide suture zone. *J. Asian Earth Sci.*, 85: 117-139.
- Göncüoğlu M.C., Turhan N., Şentürk K., Özcan A. and Uysal S., 2000. A geotraverse across NW Turkey: tectonic units of the Central Sakarya region and their tectonic evolution. In: E. Bozkurt, J. Winchester and J.A. Piper, (Eds.), *Tectonics and magmatism in Turkey and the surrounding area*. *Geol. Soc. London Spec. Publ.*, 173: 139-161.
- Güçtekin A., Köprübaşı N. and Aldanmaz E., 2004. Geochemistry of the Karabiga (Çanakale) Granitoid. *Bull. Earth Sci. Hacettepe*, 29: 29-38.
- Hall R., 1976. Ophiolite emplacement and evolution of the Taurus suture zone, southeastern Turkey. *Geol. Soc. Am. Bull.*, 87: 1078-1088.
- Hamelin B. and Allègre C.J., 1985. Large scale regional units in the depleted upper mantle revealed by an isotopic study of the south-west India ridge. *Nature*, 315: 196-198.
- Hamilton W., 1969. Mesozoic California and underflow of Pacific mantle. *Geol. Soc. Am. Bull.*, 80: 2409-2430.
- Hart S.R., 1984. The Dupal anomaly: a large-scale isotopic anomaly in the southern hemisphere. *Nature*, 309: 753-756.
- Hart S.R., 1988. Heterogeneous mantle domains: signature, genesis and mixing chronologies. *Earth Planet. Sci. Lett.*, 90: 273-296.
- Hart S.R., Gerlach D.C. and White W.M., 1986. A possible new Sr-Nd-Pb mantle array and consequences for mantle mixing. *Geochim. Cosmochim. Acta*, 50: 1551-1557.
- Hauff F., Hoernle K. and Schmidt A., 2003. Sr-Nd-Pb composition of Mesozoic Pacific oceanic crust (Site 1149 and 801, ODP Leg 185): implications for alteration of ocean crust and the input into the Izu-Bonin-Mariana subduction system. *Geochem., Geophys., Geosyst.*, 4 (8): 8913, doi:10.1029/2002GC000421.
- Hawkesworth C.J., Rogers N.W., van Calsteren P.W.C. and Menzies M.A., 1984. Mantle enrichment processes. *Nature*, 311 (27): 331-335.
- Hemond C., Hofmann A.W., Vlastelic I. and Nauret F., 2006. Origin of MORB enrichment and relative trace element compatibilities along the Mid-Atlantic Ridge between 10° and 24°N. *Geochem., Geophys., Geosyst.*, 7, doi:10.1029/2006GC001317.
- Hoek V., Ionescu C., Balintoni I. and Koller F., 2009. The Eastern Carpathians "ophiolites" (Romania): Remnants of a Triassic ocean. *Lithos*, 108: 151-171.
- Hsü K.J., 1968. Principles of mélanges and their bearing on the Franciscan-Knoxville paradox. *Geol. Soc. Am. Bull.*, 79: 1069-1074.
- Ionescu C., Hoek V., Tomek C., Koller F., Balintoni I. and Lucian B., 2009. New insights into the basement of the Transylvanian Depression (Romania). *Lithos*, 108: 172-191.
- Ionov D.A. and Hofmann A.W., 1995. Nb-Ta-rich mantle amphiboles and micas: implications for subduction-related metasomatic trace element fractionations. *Earth Planet. Sci. Lett.*, 131: 341-356.
- Kaaden G. van der, 1959. Age relations of magmatic activity and of metamorphic processes in the northwestern part of Anatolia-Turkey. *Bull. Min. Res. Explor. Int. Turkey, Foreign Edition*, 52: 15-34.
- Koçyiğit A., 1991. An example of an accretionary forearc basin from northern Central Anatolia and its implications for the history of subduction of Neo-Tethys in Turkey. *Geol. Soc. Am. Bull.*, 103: 22-36.
- Köksal S. and Göncüoğlu M.C., 2008. Sr and Nd isotopic characteristics of some S-, I- and A-type granitoids from Central Anatolia. *Turk. J. Earth Sci.*, 17: 111-127.
- Kuzmichev A., Kröner A., Hegner E., Dunyi L. and Yusheng W., 2005. The Shishkhid ophiolite, northern Mongolia: a key to the reconstruction of a Neoproterozoic island-arc system in central Asia. *Precamb. Res.*, 138: 12-150.
- LaFlèche M.R., Camiré G. and Jenner G.A., 1998. Geochemistry of post-Acadian, Carboniferous continental intraplate basalts from the Maritimes basin, Magdalen islands, Québec, Can. *Chem. Geol.*, 148: 115-136.
- Laurora A., Mazzucchelli M., Rivalenti G., Vannucci R., Zanetti A., Barbieri M.A. and Cingolani C.A., 2001. Metasomatism and melting in carbonated peridotite xenoliths from the mantle wedge: the Gobernador Gregores case (South Patagonia). *J. Petrol.*, 42: 69-87.
- Liu X., Xu J., Castillo P.R., Xia W., Shi Y., Fenga Z. and Guo L., 2013. The Dupal isotopic anomaly in the southern Paleo-Asian Ocean: Nd-Pb isotope evidence from ophiolites in Northwest China. *Lithos*, 189: 185-200.
- Marroni M., Frassi C., Göncüoğlu, M.C., Di Vincenzo G., Pandolfi, L., Rebay, G., Ellero A. and Ottria G., 2014. Late Jurassic amphibolite-facies metamorphism in the Intra-Pontide Suture Zone (Turkey): an eastward extension of the Vardar Ocean from the Balkans into Anatolia? *J. Geol. Soc.*, 171: 605-608.
- McCulloch M.T., Gregory R.T., Wasserburg G.T. and Taylor H.P., 1981. Sm-Nd, Rb-Sr, and 180/160 isotopic systematics in an oceanic crustal section: evidence from the Samail ophiolite. *J. Geophys. Res.*, 86: 2721-2735.
- Nauret F., Abouchami W., Galer S.J.G., Hofmann A.W., Hemond C., Chauvel C. and Dymant J., 2006. Correlated trace element-Pb isotope enrichments in Indian MORB along 10°-20°S, Central Indian Ridge. *Earth Planet. Sci. Lett.*, 245: 137-152.
- Nicolae I. and Saccani E., 2003. Petrology and geochemistry of the Late Jurassic calc-alkaline series associated to Middle Jurassic ophiolites in the South Apuseni Mountains (Romania). *Swiss J. Petrol.*, 83: 81-96.
- Niu Y., Collerson K.D. and Batiza R., 1999. Origin of enriched-type mid-ocean ridge basalt at ridges far from mantle plumes: the East Pacific Rise at 11°20'N. *J. Geophys. Res.* 104: 7067-7087.
- Okay A. İ., 1987. Ophiolite obduction on a Permian carbonate platform in northwest Turkey. 4<sup>th</sup> Meet. Europ. Union Geosci. (EUG IV), *Terra Cognita*, 7: 100.
- Okay A.İ. and Şahintürk Ö., 1997. Geology of the Eastern Pontides. In: A.G. Robinson (Ed.), *Regional and petroleum geology of the Black Sea and surrounding region*. AAPG Mem., 68: 291-311.
- Okay A.I. and Satır M. 2000a. Upper Cretaceous eclogite-facies metamorphic rocks from the Biga Peninsula, Northwest Turkey. *Turk. J. Earth Sci.*, 9: 47-56.
- Okay A.İ. and Tüysüz O., 1999. Tethyan Sutures of northern Turkey. In: B. Durand, L. Jolivet, F. Horvath and M. Seranne (Eds.), *Mediterranean basins: Tertiary extension within the Alpine Orogen*. *Geol. Soc. London Spec. Publ.*, 156: 475-515.
- Okay A.İ., Satır M., Maluski H., Siyako M., Monie P., Metzger R. and Akyüz S., 1996. Paleo- and Neo-Tethyan events in northwestern Turkey: geologic and geochronologic constraints. In: A. Yin and T.M. Harrison (Eds.), *The tectonic evolution of Asia*. Cambridge Univ. Press, p. 420-441.
- Okay A., Siyako M. and Bürkan K. A., 1990. Geology and tectonic evolution of the Biga Peninsula. *Bull. of the Tech. Univ. of Istanbul*, 44 (1): 191-255.
- Pearce J.A., 1982. Trace element characteristics of lavas from destructive plate boundaries: In: R.S. Thorpe (Ed.), *Andesites*. New York, J. Wiley and Sons, p. 525-548.
- Pearce J.A., 1996. A user's guide to basalt discrimination diagrams. In: D.A. Wyman (Ed.), *Trace element geochemistry of volcanic rocks: Applications for massive sulphide exploration*. *Geol. Ass. Can., Short Course Notes*, 12: 79-113.
- Pearce J. A., 2003. Supra-subduction zone ophiolites: The search for modern analogues. In: Y. Dilek and S. (Eds.), *Newcomb ophiolite concept and evolution of geological thought*. *Geol. Soc. Am. Spec. Publ.*, 373: 269-93.
- Pearce J.A., 2008. Geochemical fingerprinting of oceanic basalts with applications to ophiolite classification and the search for Archean oceanic crust. *Lithos*, 100: 14-48.

- Pearce J. and Cann J., 1973. Tectonic setting of basic volcanic rocks determined using trace element analyses. *Earth Planet. Sci. Lett.*, 19: 290-300.
- Pearce J. A. and Norry M.J., 1979, Petrogenetic implications of Ti, Zr, Y, and Nb, variations in volcanic rocks. *Contr. Mineral.*, 69: 33-47.
- Pearce J.A. and Peate D.W., 1995. Tectonic implications of the composition of volcanic arc magmas. *Ann. Rev. Earth Planet. Sci.*, 23: 251-285.
- Pearce J.A. and Stern, R.J., 2006. Origin of back-arc basin magmas: trace element and iso-tope perspectives. Back-arc spreading systems: geological, biological, chemical and physical interactions. *Geophys. Monogr. Ser.*, 166: 63-86.
- Pearce J.A., Ernewein M., Bloomer S.H., Parson L.M. Murton B.J. and Johnson L.E., 1994. Geochemistry of Lau Basin volcanic rocks: influence of ridge segmentation and arc proximity. In: J.L. Smellie (Ed.), *Volcanism associated with extension at consuming plate margins*. *Geol. Soc. London Spec. Publ.*, 81: 53-75.
- Pearce J.A., Kempton P.D., Nowell G.M. and Noble S.R., 1999. Hf-Nd element and isotope perspective on the nature and provenance of mantle and subduction components in Western Pacific arc-basin systems. *J. Petrol.*, 40: 1579-1611.
- Pearce J.A., Lippard S.J. and Roberts S., 1984. Characteristics and tectonic significance of supra-subduction zone ophiolites. In: B.P. Kokelaar and M.F. Howells (Eds.), *Marginal basin geology*. London, Blackwell Scientific, p. 77-94.
- Pickett E.A. and Robertson A.H.F., 1996. Formation of the late Palaeozoic-Early Mesozoic Karakaya complex and related ophiolites in NW Turkey by Paleotethyan subduction-accretion. *J. Geol. Soc. London*, 153: 995-1009.
- Pilet S., Hernandez J., Sylvester P. and Poujol M., 2005. The metasomatic alternative for ocean island basalt chemical heterogeneity. *Earth Planet. Sci. Lett.*, 236: 148-66.
- Robertson A.H.F. and Ustaömer T., 2004. Tectonic evolution of the Intra-Pontide suture zone in the Armutlu Peninsula, NW Turkey. *Tectonophysics*, 381: 175-209.
- Raymond L.A. and Terranova T., 1984. Prologue - the mélange problem - a review. In: L.A. Raymond (Ed.), *Mélanges: their nature, origin and significance*. *Geol. Soc. Am. Spec. Pap.*, 198: 1-5.
- Ross P.-S. and Bedard J.H., 2009. Magmatic affinity of modern and ancient sub-alkaline volcanic rocks determined from trace element discriminant diagrams. *Can. J. Earth Sci.*, 46: 823-839.
- Saccani E., 2015. A new method of discriminating different types of post-Archean ophiolitic basalts and their tectonic significance using Th-Nb and Ce-Dy-Yb systematics. *Geosci. Front.*, 6: 481-501.
- Saccani E., Bortolotti V., Marroni M., Pandolfi L., Photiades A. and Principi G., 2008. The Jurassic association of backarc basin ophiolites and calc-alkaline volcanics in the Guevgueli Complex (northern Greece): Implication for the evolution of the Vardar Zone. *Ophiolite*, 33: 209-227.
- Saunders A.D. and Tarney J., 1984. Geochemical characteristics of basaltic volcanism within back-arc basins. In: B.P. Kokelaar and M.F. Howells (Eds.), *Marginal basin geology*. *Geol. Soc. London Spec. Publ.*, 16: 59-76.
- Schmid S.M., Bernoulli D., Fugenschuh B., Matenco L., Schefer S., Schuster R., Tischler M. and Ustaszewski K., 2008. The Alpine-Carpathian-Dinaridic orogenic system: correlation and evolution of tectonic units. *Swiss J. Geosci.*, 101: 139-183.
- Seal A.E., Hart S.R., Shimizu N., Hauri E.H. and Layne G.D., 1998. Pb isotopic variability in melt inclusions from oceanic island basalts, Polynesia. *Science*, 282: 1481-1484.
- Shervais J.W., 1982. Ti-V plots and the petrogenesis of modern and ophiolitic lavas. *Earth Planet. Sci. Lett.*, 59: 101-118.
- Shervais, J.W. 2001. Birth, death, and resurrection: The life cycle of suprasubduction zone ophiolites. *Geochem. Geophys. Geosyst.* 2, GC000080, 45 pp., doi: 10.1029/2000GC000080.
- Silver E.A. and Beutner E.C., 1980. *Mélanges*. *Geology*, 8: 32-34.
- Siyako M., Bürkan K.A. and Okay A.İ., 1989. Tertiary geology and hydrocarbon potential of the Biga and Gelibolu Peninsula. *TAPG Bull.*, 1 (3): 183-199.
- Sinton J.M., Ford L.L., Chappell B. and McCulloch M.T., 2003. Magma genesis and mantle heterogeneity in the Manus back-arc basin, Papua New Guinea. *J. Petrol.*, 44: 159-195.
- Stern R.J., Lin P.-N., Morris J.D., Jackson M.C., Fryer P., Bloomer S.H. and Ito E., 1990. Enriched back-arc basin basalts from the northern Mariana Trough: implications for the magmatic evolution of back-arc basins. *Earth Planet. Sci. Lett.*, 100: 210-225.
- Sun S.S. and McDonough W.F., 1989. Chemical and isotopic systematics and processes. In: A.D. Saunderson and M.S. Norry (Eds.), *Magmatism in the ocean basins*. *Geol. Soc. London Spec. Publ.*, 42: 313-345.
- Şengör A.M.C. and Yılmaz Y., 1981. Tethyan evolution of Turkey: a plate tectonic approach. *Tectonophysics* 75: 181-241.
- Taylor B. and Martinez F., 2003. Back-arc basin basalt systematics. *Earth Planet. Sci. Lett.*, 210: 481-497.
- Thirlwall M.F., Smith T.E., Graham A.M., Theodorou N., Hollings P., Davidson J.P. and Arculus R.J., 1994. High field strength element anomalies in arc lavas: source or process? *J. Petrol.*, 35: 819-838.
- Weaver B.L., 1991. The origin of ocean island basalt end-member compositions: trace element and isotopic constraints. *Earth Planet. Sci. Lett.*, 104: 381-397.
- Wong K., Sun M., Zhao G., Yuan C. and Xiao W., 2010. Geochemical and geochronological studies of the Alegendayi Ophiolitic Complex and its implication for the evolution of the Chinese Altai. *Gondwana Res.*, 18: 438-454.
- Wood D.A., 1980. The application of a Th-Hf-Ta diagram to problems of tectonomagmatic classification and to establishing the nature of crustal contamination of basaltic lavas of the British Tertiary volcanic province. *Earth Planet. Sci. Lett.*, 50: 11-30.
- Woodhead J., Eggins S. and Gamble J., 1993. High field strength and transition element systematics in island arc and back-arc basin basalts: evidence for multi-phase melt extraction and a depleted mantle wedge. *Earth Planet. Sci. Lett.*, 114: 491-504.
- Yılmaz Y., Tüysüz O., Yigitbas E., Genç S.C. and Şengör A.M.C., 1997. Geology and tectonic evolution of the Pontides. In: A.G. Robinson (Ed.), *Regional and petroleum geology of the Black Sea and surrounding region*. *Bull. Am. Ass. Petr. Geol.*, 68: 183-226.
- Yiğitbaş E., Elmas A. and Yılmaz Y., 1999. Pre-Cenozoic tectonostratigraphic components of the Western Pontides and their geological evolution. *Geol. J.*, 34: 55-74.

Received, February 26, 2018

Accepted, June 12, 2018